A guiding role of the Arabidopsis circadian clock in cell differentiation revealed by time-series single-cell RNA sequencing

AUTHOR(S):

Torii, Kotaro; Inoue, Keisuke; Bekki, Keita; Haraguchi, Kazuya; Kubo, Minoru; Kondo, Yuki; Suzuki, Takamasa; ... Fukuda, Hiroo; Araki, Takashi; Endo, Motomu

CITATION:

Torii, Kotaro ...[et al]. A guiding role of the Arabidopsis circadian clock in cell differentiation revealed by time-series single-cell RNA sequencing. Cell Reports 2022, 40(2): 111059.

ISSUE DATE:

2022-07-12

URL:

http://hdl.handle.net/2433/276853

Article

Cell Reports

A guiding role of the *Arabidopsis* circadian clock in cell differentiation revealed by time-series single-cell RNA sequencing

Graphical abstract

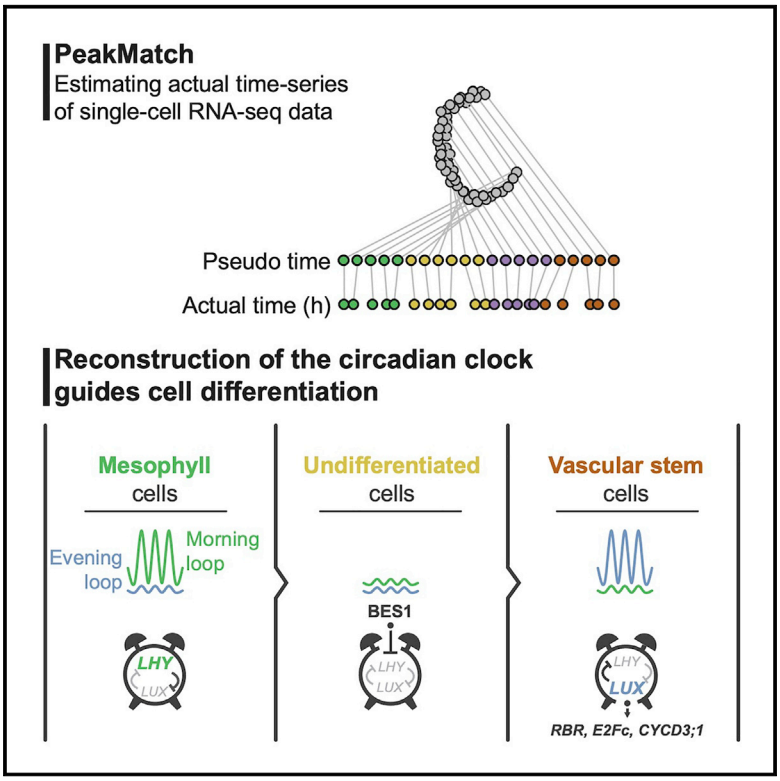

Authors

Kotaro Torii, Keisuke Inoue, Keita Bekki, ..., Hiroo Fukuda, Takashi Araki, Motomu Endo

Correspondence

endo@bs.naist.jp

In brief

Circadian rhythms generated by the circadian clock regulate various physiological responses, including cell differentiation. Torii et al. show that circadian rhythms are disrupted in reprogrammed cells, whereas construction of circadian rhythms with tissue-specific expression profiles of clock genes regulates the cell cycle to guide cell differentiation.

Highlights

- Perturbations in circadian rhythms reduce frequency of cell differentiation
- Expression of all clock genes is less periodic in reprogrammed cells
- Expression of *ELF4* and *LUX* is induced prior to cell differentiation
- LUX directly regulates cell-cycle-related genes in differentiating cells

Torii et al., 2022, Cell Reports *40*, 111059
July 12, 2022
https://doi.org/10.1016/j.celrep.2022.111059

CellPress

Cell Reports

CellPress OPEN ACCESS

Article

A guiding role of the *Arabidopsis* circadian clock in cell differentiation revealed by time-series single-cell RNA sequencing

Kotaro Torii,[1,2,8] Keisuke Inoue,[1,8] Keita Bekki,[1,2] Kazuya Haraguchi,[3] Minoru Kubo,[4] Yuki Kondo,[5,6] Takamasa Suzuki,[7] Akane Kubota,[2] Kyohei Uemoto,[1,2] Hanako Shimizu,[1] Masato Saito,[5] Hiroo Fukuda,[5] Takashi Araki,[1] and Motomu Endo[2,9,*]

[1]Division of Integrated Life Science, Graduate School of Biostudies, Kyoto University, Sakyo-ku, Kyoto 606-8501, Japan
[2]Graduate School of Science and Technology, Nara Institute of Science and Technology, Ikoma, Nara 630-0192, Japan
[3]Department of Applied Mathematics and Physics, Kyoto University, Kyoto 606-8501, Japan
[4]Graduate School of Science and Technology, Kumamoto University, 2-39-1 Kurokami, Chuo-ku, Kumamoto 860-8555, Japan
[5]Department of Biological Sciences, Graduate School of Science, The University of Tokyo, 7-3-1 Hongo, Bunkyo-ku, Tokyo 113-0033, Japan
[6]Department of Biology, Graduate School of Science, Kobe University, Kobe 657-8501 Japan
[7]Department of Biological Chemistry, College of Bioscience and Biotechnology, Chubu University, Kasugai, Aichi 487-8501, Japan
[8]These authors contributed equally
[9]Lead contact
*Correspondence: endo@bs.naist.jp
https://doi.org/10.1016/j.celrep.2022.111059

SUMMARY

Circadian rhythms and progression of cell differentiation are closely coupled in multicellular organisms. However, whether establishment of circadian rhythms regulates cell differentiation or vice versa has not been elucidated due to technical limitations. Here, we exploit high cell fate plasticity of plant cells to perform single-cell RNA sequencing during the entire process of cell differentiation. By analyzing reconstructed actual time series of the differentiation processes at single-cell resolution using a method we developed (PeakMatch), we find that the expression profile of clock genes is changed prior to cell differentiation, including induction of the clock gene *LUX ARRYTHMO* (*LUX*). ChIP sequencing analysis reveals that LUX induction in early differentiating cells directly targets genes involved in cell-cycle progression to regulate cell differentiation. Taken together, these results not only reveal a guiding role of the plant circadian clock in cell differentiation but also provide an approach for time-series analysis at single-cell resolution.

INTRODUCTION

The circadian clock was selected for a mechanism to control cell-cycle progression to avoid sunlight-induced DNA damage in ancient unicellular organisms (Hut and Beersma, 2011). Presumably for this reason the circadian clocks in multicellular organisms are involved in both cell-cycle progression and the associated cell fate transitions (Weger et al., 2017; Tsuchiya et al., 2020). In mammalian embryonic stem cells, circadian rhythms are not observed during early developmental stages but emerge with cell differentiation; and the circadian rhythms in differentiated cells disappear when they are reprogrammed (Kowalska et al., 2010; Yagita et al., 2010; Paulose et al., 2012; Dierickx et al., 2018). Furthermore, several mutations in clock genes cause abnormal cell differentiation in mammals (Yu et al., 2013; Dierickx et al., 2018). Similarly in *Arabidopsis*, a double mutant of *CIRCADIAN CLOCK ASSOCIATED 1* (*CCA1*) and *LATE ELONGATED HYPOCOTYL* (*LHY*) has defects in vein pattern with an increased number of free-ending vascular bundles, suggesting a link between the circadian clock and cell differentiation (Aihara et al., 2014). Therefore, elucidating how the circadian clock is involved in cell differentiation is important to understand the basis of cell fate determination and the time-series analysis of gene expression dynamics during cell differentiation at single-cell resolution is a promising approach.

Single-cell RNA sequencing (scRNA-seq) with unique molecular identifiers (UMI) (Islam et al., 2014) combined with bioinformatics toolkits such as Wishbone (Setty et al., 2016) and Seurat (Satija et al., 2015) have been used to study the differentiation process from stem cells, and a pseudo-time trajectory from scRNA-seq datasets enables us to estimate changes in transcriptome profiles during the developmental process. Using these techniques, developmental cell lineage has been intensively studied with high spatial resolution, especially in animal stem cells. However, a single-cell transcriptome analysis during cell differentiation is still difficult in plant cells because single-cell isolation usually requires a time-consuming process such as cell wall digestion. Furthermore, the timescale in the pseudo-time analysis is literally "pseudo." and it was challenging to perform a temporal analysis that required correspondence with actual time such as circadian rhythms. This lack of analysis from a time perspective has

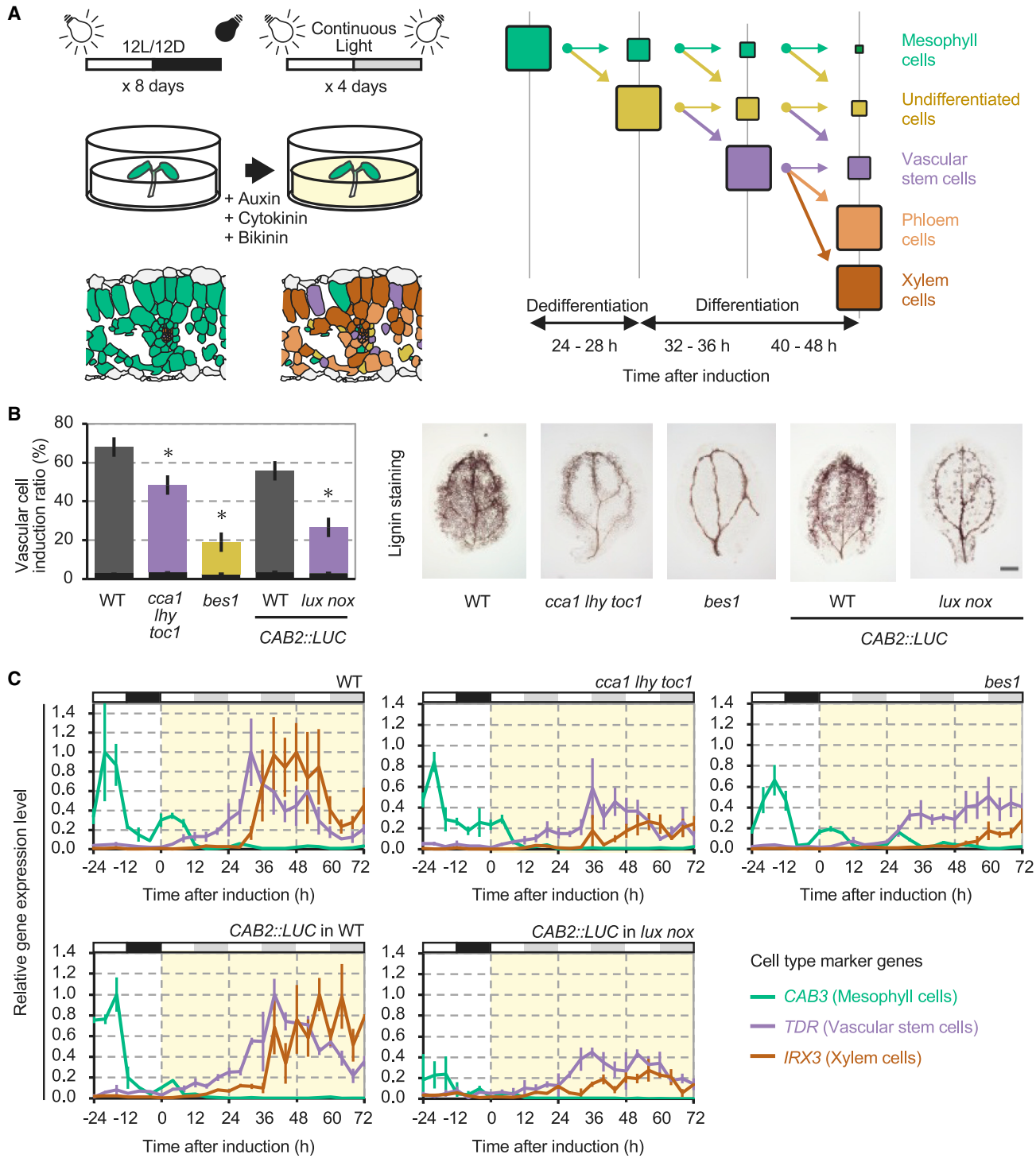

Figure 1. Involvement of the plant circadian clock in the cell differentiation process

(A) Schematic illustration of ectopic vascular cell induction with VISUAL. The size of the square schematically represents the proportion of cells. See also Figure S1A.

(B) Lignin-stained xylem cell density in WT, *cca1 lhy toc1*, *lux nox*, and *bes1* 96 h after differentiation induction. Gray and colored bars indicate ectopically induced xylem cells, and black bars indicate endogenous xylem cells (left, n = 5 cotyledons, mean ± SEM, Dunnett's test, *p < 0.05). Representative photos of lignin staining (right, bar = 0.5 mm). See also Figures S1B–S1I.

(legend continued on next page)

delayed our understanding of molecular roles of the circadian clock in cell differentiation from stem cells.

Here, we focused on a differentiation induction system of *Arabidopsis* that can analyze the entire process of cell differentiation, taking advantage of high cell fate plasticity in plants. Using this system, we performed *in vivo* scRNA-seq without single-cell isolation and analyzed the cell differentiation process with high spatiotemporal resolution using a newly developed method for reconstruction of actual-time series. This study not only elucidated a molecular basis of the plant circadian clock for cell differentiation but also provided a novel approach for a time-series single cell transcriptome analysis.

RESULTS

Involvement of the plant circadian clock in the cell differentiation process

To investigate whether the plant circadian clock is involved in cell differentiation processes, we utilized VISUAL, a vascular cell differentiation induction system in *Arabidopsis* (Kondo et al., 2014, 2016). In this system, mesophyll cells dedifferentiate immediately after differentiation induction, and resulting reprogrammed cells differentiate into vascular cells (including both xylem and phloem cells) within 3 days (Figures 1A, S1A, and S1B). Although clear circadian rhythms were observed in the original protocol (Kondo et al., 2016), it used continuous-light conditions for growing plants (Figure S1C). We here adopted the condition of 12L12D (12 h light and 12 h dark) for pre-culture to sustain robust circadian rhythms and constant light for VISUAL to precisely monitor changes in circadian rhythms upon the induction of differentiation. In order to ensure disruption of the functional circadian clock, we used multiple mutants of clock genes in addition to single mutants of each clock gene for analyses. Two multiple clock mutants, a triple mutant of *CCA1*, *LHY*, and *TIMING OF CAB EXPRESSION 1* (*TOC1*) referred to as *cca1 lhy toc1* and a double knockdown of *LUX ARRHYTHMO* (*LUX*)/*PHYTOCLOCK 1* and *BROTHER OF LUX ARRHYTHMO* (also known as *NOX*) by artificial microRNA referred to as *lux nox* (Helfer et al., 2011), and single mutants for *CCA1*, *LHY*, and *TOC1* showed significant defects in vascular cell differentiation (Figures 1B and S1D–S1F), similarly to a loss-of-function mutant of *BRI1-EMS SUPPRESSOR 1* (*BES1*), which shows severe defects in vascular cell differentiation in VISUAL (Kondo et al., 2014). Since several independent mutants of the clock genes showed similar phenotypes, we hypothesized that proper circadian rhythms are important for cell differentiation. To test this hypothesis, we examined the effect of perturbations in circadian rhythms on vascular cell differentiation. Attenuation of circadian rhythms by random light/dark conditions inhibited vascular cell differentiation in wild type (WT), whereas further reduction of vascular cell differentiation was not observed in the *lux nox* (Figures S1G and S1H). In addition, *LHY*-overexpressing plants, which exhibit arrhythmia of circadian rhythms (Schaffer et al., 1998), showed similar defects in vascular differentiation as observed in *cca1 lhy toc1* (Figure S1I), suggesting that robust circadian rhythms, not clock genes themselves, are significant for vascular cell differentiation. Furthermore, consistent with the previous observation in a *cca1 lhy* (Aihara et al., 2014), the *cca1 lhy toc1* and the *lux nox* showed abnormal patterns of vascular bundles with increased free ends in the non-VISUAL condition (Figures S1J–S1L), although the cotyledons in the *cca1 lhy toc1* did not show any significant difference in the condition (Figure S1L). We also confirmed that the clock mutants showed reduced stomatal indices and root growth in non-VISUAL conditions (Figures S1M and S1N). These results suggest that the circadian clock is generally involved in the process of cell differentiation not only in artificial VISUAL but also in natural non-VISUAL conditions.

The VISUAL assay consists of two steps: dedifferentiation of mesophyll cells into reprogrammed cells and differentiation of the reprogrammed cells into vascular cells (Yamazaki et al., 2018). To determine which step is regulated by the circadian clock, we first measured expression levels of cell-type-specific markers. In WT, the expression of mesophyll cell markers (*CAB3* and *LHCB2.1*) (Endo et al., 2014) disappeared after differentiation induction, followed by induction of vascular stem cell markers (*TDR* and *ANT*) (Kondo et al., 2014; Campbell and Turner, 2017) and vascular cell markers (*IRX3* and *VND7*) (Yamaguchi et al., 2011) (Figures 1C and S2). This trajectory of cell differentiation was consistent with a series of previous reports (Kondo et al., 2014, 2016). We next examined how mutations in the clock genes affect the trajectory of cell differentiation. In the *cca1 lhy toc1* and the *lux nox* as well as the *bes1*, circadian oscillation of mesophyll cell markers declined over time after differentiation induction as in the WT, suggesting that the dedifferentiation process was not inhibited in these mutants (Figures 1C and S2). By contrast, the induction of vascular stem cell markers and xylem cell markers were not comparable to the expression levels of the WT (Figures 1C and S2). Taken together, these results suggest that the circadian clock as well as BES1 are involved in the process of cell differentiation rather than dedifferentiation.

BES1 directly suppressed *LHY* expression during cell differentiation

BES1 plays a pivotal role in the regulation of both cell proliferation and cell differentiation (Li et al., 2018), and vascular cell differentiation in VISUAL is severely inhibited in the *bes1* mutant (Figure 1B; Kondo et al., 2014; Saito et al., 2018). BES1 has two forms: a physiologically inactive phosphorylated form and a physiologically active dephosphorylated form (Sharma et al., 2014). The active form of dephosphorylated BES1 was highly accumulated immediately after differentiation induction (Figure 2A). Since a previous study had shown that BES1 directly suppressed the expression of *LHY* (Yu et al., 2011), we hypothesized that perturbations to the circadian clock by BES1 might trigger the differentiation of vascular stem cells from reprogrammed cells. To test the hypothesis, we performed chromatin immunoprecipitation (ChIP)-qPCR and confirmed the enrichment of BES1-GFP at the G-box and E-box motifs in the *LHY*

(C) Expression patterns of cell-type-specific markers during VISUAL in WT, *cca1 lhy toc1*, *lux nox*, and *bes1* (n = 3 cotyledons, mean ± SEM). Green, purple, and red lines indicate marker genes for mesophyll cells (*CAB3*), vascular stem cells (*TDR*), and xylem cells (*IRX3*), respectively. Expression peaks of each respective gene in WT were normalized to 1. White, black, and gray boxes indicate light period, night period, and subjective night period, respectively. See also Figure S2.

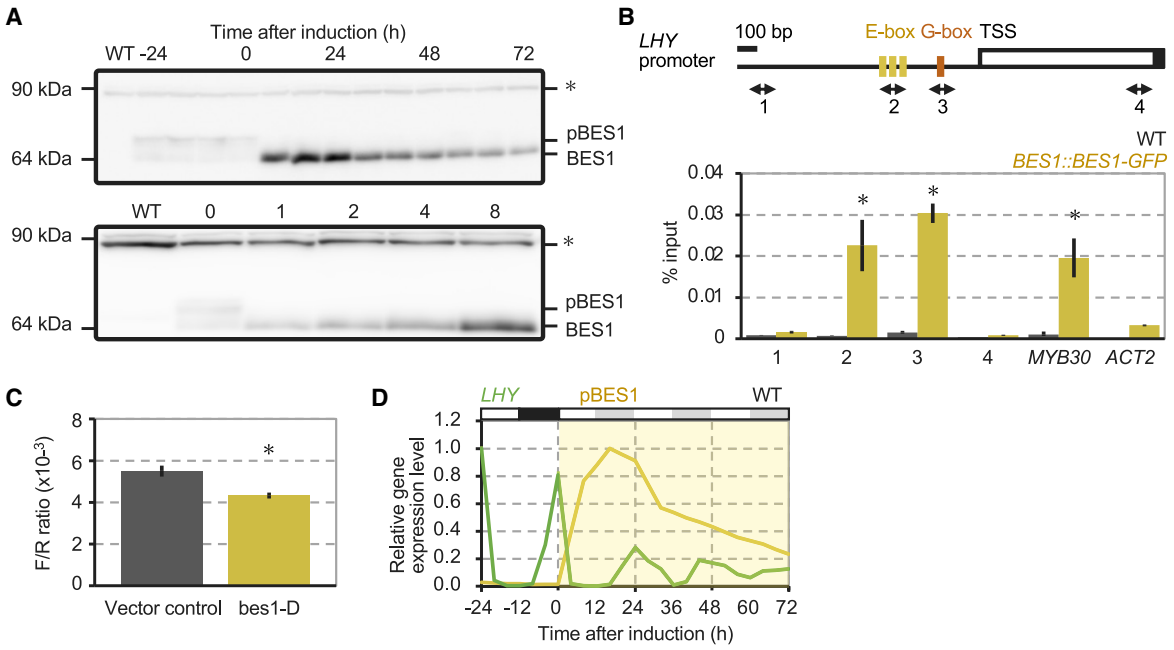

Figure 2. BES1 directly suppressed *LHY* expression during cell differentiation

(A) Immunoblot analyses of BES1-GFP proteins during VISUAL. Samples were harvested every 8 h, from 24 h before up to 72 h after differentiation induction (top) and from 0 to 8 h after differentiation induction (bottom). pBES1 indicates phosphorylated BES1. Asterisks indicate non-specific bands.

(B) ChIP-qPCR analyses using WT and *BES1:BES1-GFP* (n = 3 cotyledons, mean ± SEM, two-sided Student's t test with Bonferroni correction, $p < 0.05$). Samples were harvested at 8 h after differentiation induction. *MYB30* and *ACT2* were used as positive and negative controls, respectively. Yellow and orange boxes indicate E-box (CANNTG) and G-box (CACGTG) motifs. TSS, transcriptional start site.

(C) Expression of *LHY:LUC* using *35S:bes1-D* as an effector in *Nicotiana benthamiana* (n = 5 leaves, mean ± SEM, two-sided Student's t test, $p < 0.05$). *35S:RLUC* was used as a transformation control. F/R ratio indicates ratio of firefly and Renilla luciferase activities.

(D) Expression pattern of *LHY* in the whole-cotyledon samples during VISUAL (n = 3 cotyledons, mean ± SEM). Relative dephosphorylated BES1 levels determined from Figure 2A are overlaid in yellow.

promoter at 8 h after differentiation induction (Figure 2B). The luciferase activity of *LHY:LUC* was decreased by transient co-expression of *bes1-D*, a gain-of-function mutant protein (Yin et al., 2002), suggesting that BES1 acts as a repressor of *LHY* expression (Figure 2C). The timing of the accumulation of activated dephosphorylated BES1 was consistent with the timing of the suppression of *LHY* expression (Figure 2D). Overall, both BES1 and LHY regulate the differentiation process, and BES1 directly suppresses *LHY* expression during differentiation induction, implying that the *LHY* regulation by BES1 is at least partly involved in the process of cell differentiation.

Reconstruction of actual time series of scRNA-seq data throughout the entire process of cell differentiation

Cell differentiation events induced by VISUAL show a high level of cell synchrony (Kondo et al., 2016). Even in this differentiation induction system, however, the timing of cell differentiation was not completely synchronized, as the expression of cell-type-specific markers overlaps (Figures 1C and S2), and the induction of vascular cells progressively increases (Figures S1B and S1D). To circumvent this low spatiotemporal resolution of bulk analyses and to elucidate when and how the circadian clock induces cell differentiation, we performed a time series of scRNA-seq. Although protoplast preparation and nuclear isolation are conventional methods for performing scRNA-seq in plants (Nelms and Walbot, 2019; Ryu et al., 2019; Shulse et al., 2019), they are time-consuming and potentially stress inducing; therefore, they are not suitable for time-series analysis of the circadian clock. For this reason, we used glass capillaries to directly acquire cell contents *in vivo* (Kubo et al., 2019). We harvested approximately seven single-cell samples every 4 h from 24 h before up to 84 h after differentiation induction (216 single cells in total) and performed scRNA-seq (Figure S3A; Table S1A; Video S1). Even when the samples were kept in the glass capillary for 600 s, the values of Pearson's correlation coefficient compared with the sample in time 0 were not decreased (Figure S3B), showing no significant degradation of mRNA during the sampling. By normalizing the scRNA-seq data with the time series of cell population RNA sequencing (cpRNA-seq) data obtained from whole cotyledons, we confirmed that expression levels of *RD29A*, a stress-inducible gene, showed no difference between the scRNA-seq and the cpRNA-seq data (Figure S3C), suggesting that our approach is not stressful. Furthermore, consistent with the notion that the timing of cell differentiation was not completely synchronized in VISUAL (Figures 1C, S1B, S1D, and S2), the values of Pearson's correlation coefficient between samples in the same time points became smaller after differentiation induction (Figure S3D). This result indicates the heterogeneity of cell differentiation in VISUAL and further supports the need for the time-series scRNA-seq.

To analyze xylem and phloem cell lineages separately, we first applied the Wishbone method, which can generate a pseudo-time trajectory from scRNA-seq data with bifurcating developmental trajectories based on an unsupervised clustering (Setty et al., 2016). t-Distributed stochastic neighbor embedding (t-SNE) of the dataset was represented by a Y-shaped structure, suggesting that the Wishbone can properly reconstruct developmental trajectories of xylem and phloem cells as expected (Figure S4A). This assertion was further validated by overlaying expression levels of cell-type-specific markers and gene ontology (GO) enrichment analysis (Figures 3A, S4B, and S4C). For simplicity, we focused on the xylem cell lineage and applied the Seurat method (Satija et al., 2015) to improve temporal resolution of the pseudo-time trajectory. Seurat estimates the order of cells on a pseudo-time series with high accuracy by referring to the expression patterns of known cell-type-specific markers (Figure S5A; Table S2).

Actual time series with interval scaling contains temporal information, whereas ordinal-scaling-based pseudo-time series lacks temporal information. Thus, time-series analysis in scRNA-seq remains a challenging task (Sun et al., 2017). To overcome this limitation and to reconstruct actual time series from single-cell transcriptome datasets, we newly developed the PeakMatch method. The basic concept of PeakMatch is to match the timing of gene expression peaks between scRNA-seq data based on pseudo-time series and cpRNA-seq data based on actual-time series, thereby conferring actual-time information to the pseudo-time series (Figures S5A and S5B). By integrating estimated peak times of 2,217 genes (Table S3; see STAR Methods and Methods S1 for details), we reconstructed actual-time-series scRNA-seq data with four cellular states comparable to the cell differentiation process observed in a previous report (Yamazaki et al., 2018) and our bulk analyses (Figures 1A, 1C, and S2; Table S1B). These clusters also included individual marker genes, supporting the validity of the clustering (Figure 3B). The half-value width of the gene expression peaks in the reconstructed actual-time series was narrow compared with that of cpRNA-seq (Figure 3C), demonstrating that PeakMatch reduces the bad averaging effect and improves temporal resolution. Furthermore, we compared PeakMatch with iCpSc (Sun et al., 2017) for estimation of actual-time information. We note that comparison of "accuracy" between algorithms is difficult because there are no numerical criteria to evaluate the quality of an estimation. To compare the accuracy between PeakMatch and iCpSc, we used each method to estimate actual time of our dataset and the dataset used in the previous report (Sun et al., 2017). In terms of coefficient of determination (R^2), PeakMatch outperformed iCpSc in both datasets (Figures S5C, S5D, and S5E). Thus, the Wishbone-Seurat-PeakMatch pipeline (Figure S5A) improved spatiotemporal resolution of scRNA-seq data and enabled us to handle actual-time-series data at single-cell resolution.

LUX in early differentiating cells binds to the promoter regions of genes involved in cell-cycle progression

Despite the fact that clock genes were not used for the reconstruction of the actual-time series, we confirmed that the expression of *LHY* and *CCA1* showed the 24-h oscillation in the differentiating/differentiated cells (Figure 3D), showing the usefulness of the PeakMatch. By contrast, the intervals of *CCA1* and *LHY* rhythms showed a longer circadian period (36 h) in the reprogrammed cells. To determine whether this phenomenon is also observed for circadian clock genes with other phases, we next analyzed periodicity of the major clock genes by a heatmap. All the clock genes are less periodic in the reprogrammed cells (Figure 3E), suggesting that the reprogrammed cells lack clear circadian oscillations.

The cease of circadian rhythm in reprogrammed cells has been similarly observed in mammalian ES/iPS cells (Kowalska et al., 2010; Yagita et al., 2010; Paulose et al., 2012; Dierickx et al., 2018). As dedifferentiation resulted in loss of mesophyll cell identity, expression of *PSEUDO-RESPONSE REGULATOR 5* (*PRR5*) and *PRR7* was diminished, and only slight expression was detected in vascular stem cells and vascular cells (Figure 4A). On the other hand, expression of *EARLY FLOWERING 4* (*ELF4*) and *LUX*, components of the evening complex (EC), which is a core transcriptional repressor complex of the plant circadian clock (Nusinow et al., 2011), was low in mesophyll cells but was significantly induced before vascular stem cell state (Figure 4A). This tendency was also seen in the correlation coefficient between clock genes and differentiation markers (Figure 4B). *LHY*, *CCA1*, *PRR5*, *PRR7*, and *PRR9* were highly correlated with mesophyll markers, whereas *ELF4* and *LUX* tended to be correlated with reprogrammed cell or vascular stem cell markers. Since LHY regulates the expression of *ELF4* and *LUX* (Li et al., 2011; Nusinow et al., 2011) and the differentiation induction is inhibited in both *bes1* and *cca1 lhy toc1* mutants (Figure 1B), the BES1-LHY pathway could explain the induction of *LUX* expression in the reprogrammed cells. Given that BES1 acts as an integrated hub in plant growth and development (Li et al., 2018) and that the circadian clocks perceive various inputs, our data do not rule out the possibility that BES1 and additional factors regulate induction of *LUX* expression through other pathways.

Predominant expression of *ELF4* and *LUX* in the differentiating cells implies specific functions of EC there. To elucidate direct targets of LUX in the differentiating cells, we then performed ChIP-seq using the LUX-GFP-expressing plants with VISUAL and detected 5,476 peaks as potential LUX targets in the differentiating cells (Table S4A). Consistent with previous ChIP-seq data using whole seedlings (Ezer et al., 2017), LUX bound to the promoters of other clock components (Table S4B). From the ChIP-seq data, we found that genes involved in cell-cycle progression, such as *CYCLIN D3;1* (*CYCD3;1*), *RETINOBLASTOMA-RELATED* (*RBR*), and *E2FC*, were significantly enriched (Figures 4C and 4D; Table S4C). Since they all are key regulators for G1 to S phase transition (De Veylder et al., 2007), this finding raises the possibility that LUX controls cell-cycle progression to regulate cell differentiation.

LUX in early differentiating cells fine-tunes cell-cycle progression during cell differentiation

Kinetics of GO-term enrichment scores throughout time course was next calculated to examine what biological process occurs during differentiation (Figure 5A). Consistent with the ChIP-seq data, GO-term related to cell-cycle progression was significantly enriched soon after the induction of *ELF4* and *LUX* (Figure 5A; highlighting in pale blue). In addition, the enrichment of

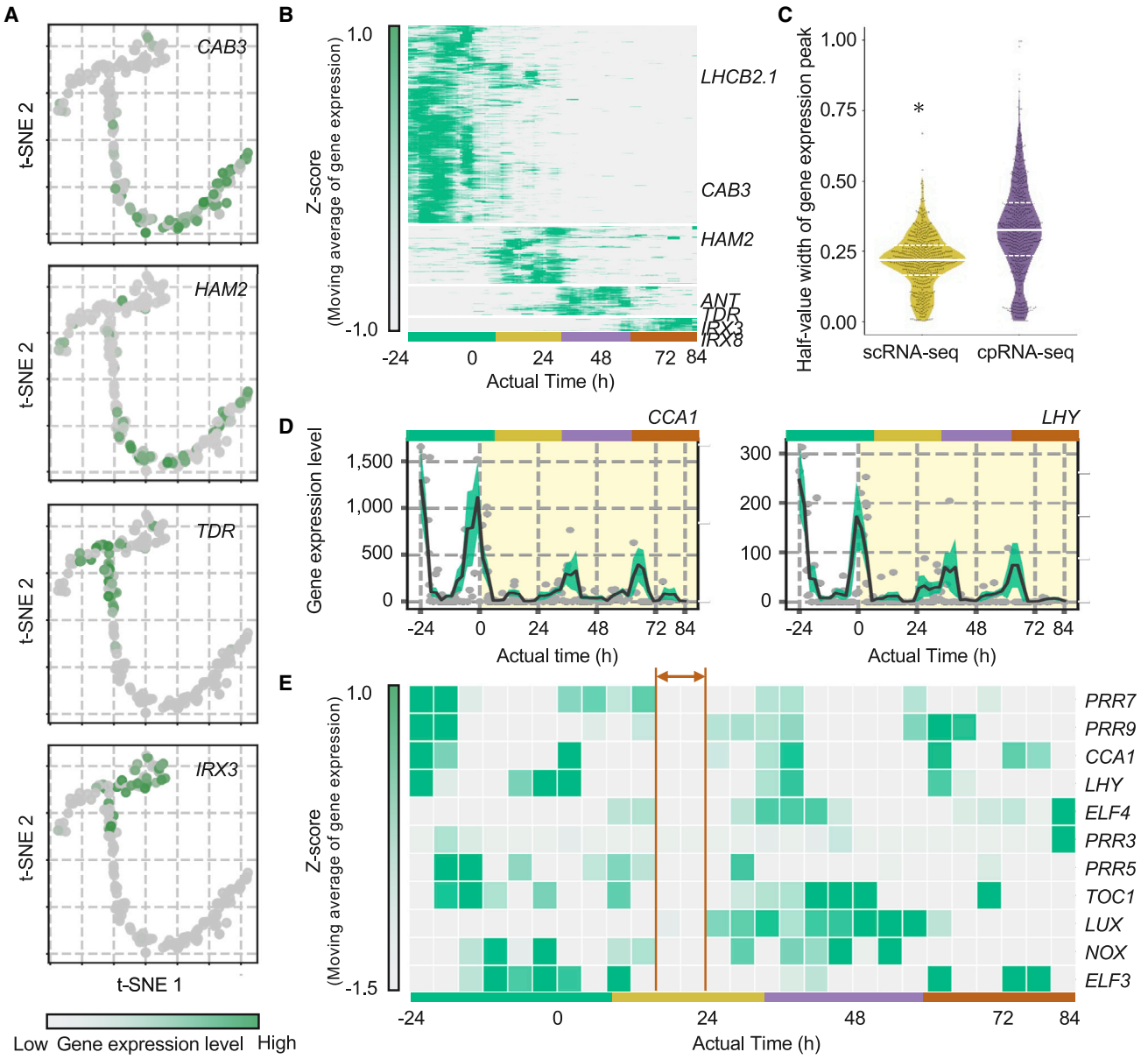

Figure 3. Reconstruction of actual-time series of scRNA-seq data throughout the entire process of cell differentiation

(A) Bifurcated cell lineage on t-SNE 2D plots predicted by Wishbone overlaid by expression levels of cell-type-specific markers. Color codes indicate normalized UMI counts from low (gray) to high (green). See also Figures S4A and S4B.

(B) A hierarchically clustered heatmap visualizing z-scores of moving averages of gene expression levels with a window size of 4 h. Green, yellow, purple, and red bars indicate marker genes for mesophyll cells, reprogrammed cells, vascular stem cells, and xylem cells, respectively. See also Figures S2 and S4C.

(C) Comparison of half-vale width of gene expression peaks between the actual time-series scRNA-seq data and the cpRNA-seq data (F test, *$p < 0.05$). White solid lines indicate the median. White broken lines indicate the upper and lower quartiles.

(D) Reconstruction of 24-h periodicity in time-series scRNA-seq by the Wishbone-Seurat-PeakMatch pipeline. Green, yellow, purple, and red bars indicate mesophyll cell, reprogrammed cell, vascular stem cell, and xylem cell states, respectively. Black solid lines are moving average of 2 h before and after. Green clouds are moving standard errors. Gray circles represent each single-cell datum.

(E) Heatmap visualizing z-scores of moving averages of each clock gene expression level with window size of 4 h. Double-headed arrow indicates a period of time when clock genes show lower amplitude in the reprogrammed cell states. Green, yellow, purple, and red bars indicate periods of time corresponding to mesophyll cell, reprogrammed cell, vascular stem cell, and xylem cell states, respectively. See also Figures S3, S4, and S5; Tables S1, S2, and S3; Video S1; and Methods S1.

GO-term DNA methylation, which could reflect initiation of cell differentiation, largely overlapped with the induction of *ELF4* and *LUX*. Notably, changes in the expression profiles of the clock genes, including the induction of *ELF4* and *LUX* expression, occurred more than 24 h before the peak of GO-terms associated with secondary cell wall biosynthesis, which

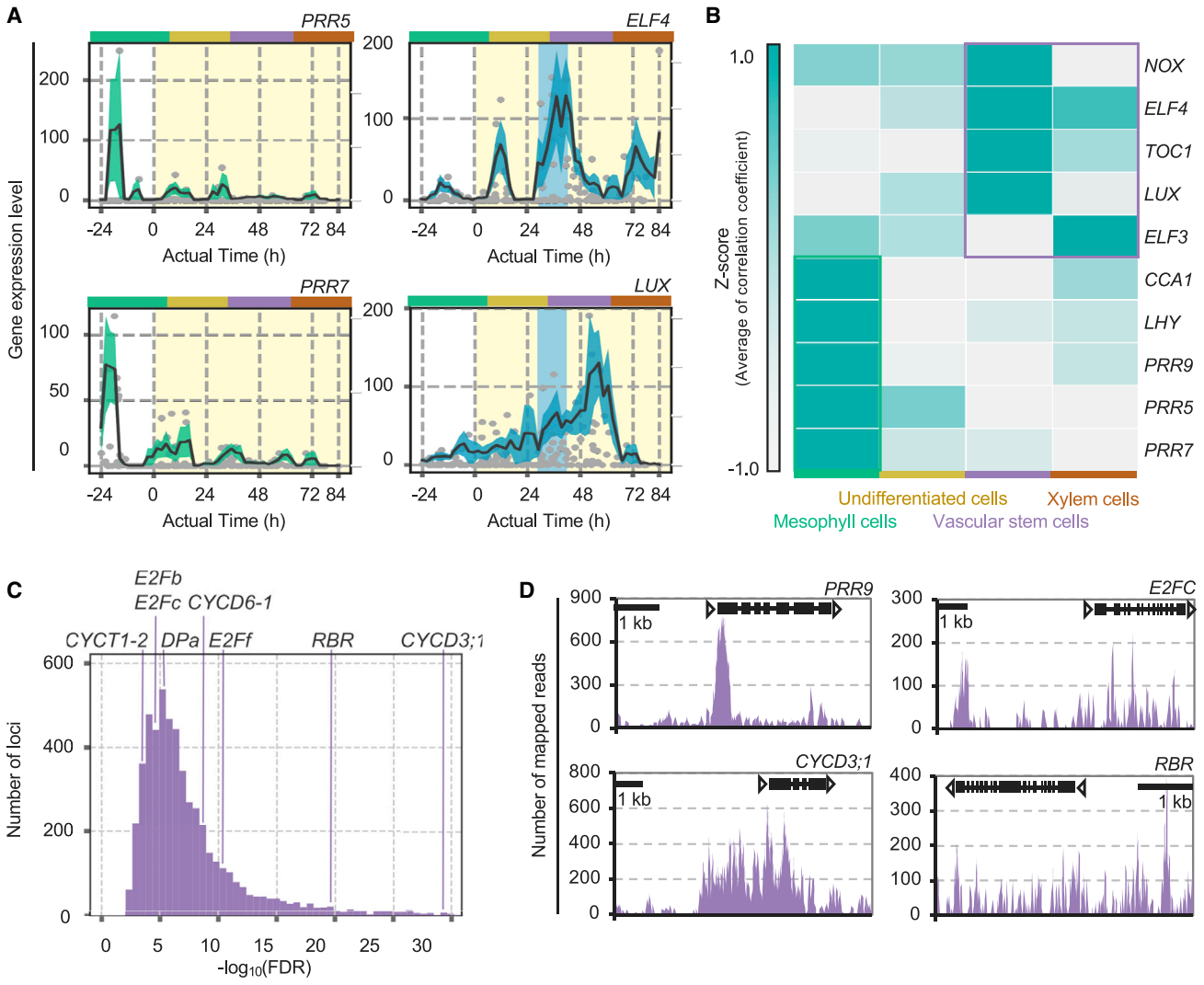

Figure 4. LUX in early differentiating cells binds to the promoter regions of genes involved in cell-cycle progression

(A) Expression patterns of clock genes in actual-time-series scRNA-seq data. Green, yellow, purple, and red bars indicate mesophyll cell, reprogrammed cell, vascular stem cell, and xylem cell states, respectively. Black solid lines are moving average of 2 h before and after. Colored clouds are moving standard errors. Gray circles represent each single-cell datum. The first peak time of *ELF4* and *LUX* expression is highlighted by the pale blue window.

(B) Pearson's correlation coefficient between clock genes and averaged cell-type-specific genes in Figure 3B.

(C) Histogram of the false discovery rates (FDR) of all potential LUX-binding loci obtained by MACS2. The positions of genes related to G1/S transition in the candidate LUX target genes are shown. *LUX:LUX-GFP/lux-4* was harvested at 24 h after differentiation induction. See also Table S4C.

(D) Visualization of ChIP-seq data around genes related to cell-cycle progression (bar, 1 kb). Genomic region around *PRR9*, a known LUX target, is shown as positive control. Peak counts of reads are shown. See also Table S4.

indicates completion of vascular cell differentiation (Figure 5A). This result suggests that establishment of circadian rhythms could predate cell differentiation, although clear 24-h oscillation was observed only in *LHY* and *CCA1* expression, probably because it is still in the process for formation of circadian rhythms. Consistently, the *lux nox* mutant affected expression of *CYCD3;1* and *E2FC* after the later stage of reprogrammed cells (36 h; Figure 5B). The lower and higher expression levels of *CYCD3;1* and *E2FC*, respectively, in the *lux nox* mutant suggest the downregulation of cell-cycle progression. To confirm the regulation of cell-cycle progression by the circadian clock, we then measured DNA ploidy levels before and after differentiation induction. DNA ploidy levels are regulated by CYCD3 and E2FC (Dewitte et al., 2007; de Jager et al., 2009) and are closely related to the progression of differentiation (Harashima and Schnittger, 2010). As expected from the expression patterns of *CYCD3;1* and *E2FC* (Figure 5B), DNA ploidy levels were increased in the clock mutants after differentiation induction (Figure 5C). Taken together, these results suggest that the changes in expression profiles of the clock genes, most notably *LUX*, in early differentiating cells fine-tune key factors for cell-cycle progression, probably leading to cell differentiation.

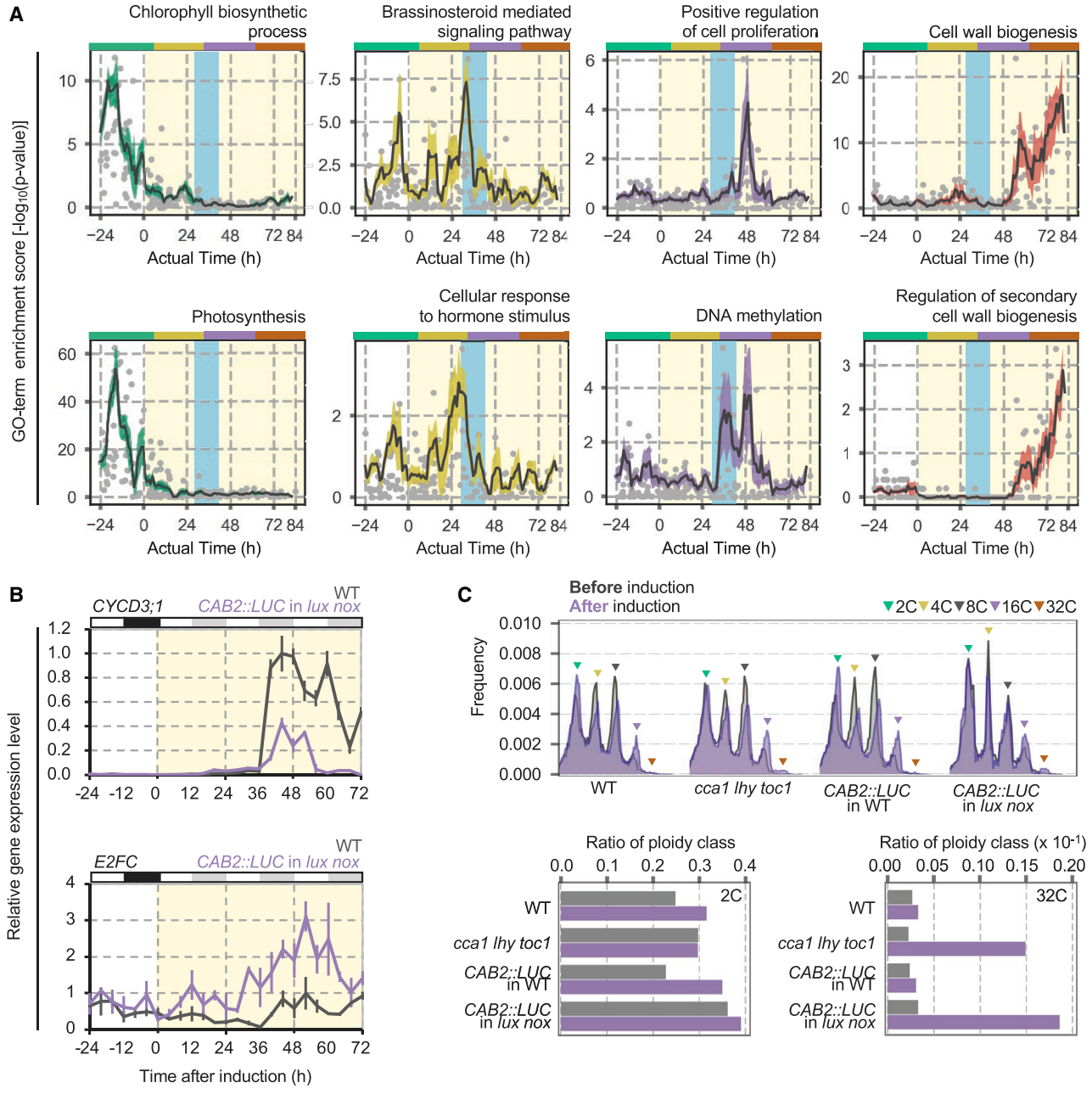

Figure 5. LUX in early differentiating cells fine-tunes cell-cycle progression to regulate cell differentiation

(A) GO term enrichment during cell fate transition. The first peak time of *ELF4* and *LUX* expression is highlighted by the pale blue window. Green, yellow, purple, and red bars indicate mesophyll cell, reprogrammed cell, vascular stem cell, and xylem cell states, respectively. Black solid lines are moving average of 2 h before and after. Colored clouds are moving standard errors. Gray circles represent each single-cell datum.

(B) Expression patterns of *CYCD3;1* and *E2FC* during VISUAL in *lux nox* and corresponding WT (n = 3 cotyledons, mean ± SEM). Peak expression levels of each respective gene in WT were normalized to 1. White, black, and gray boxes indicate light period, night period, and subjective night period, respectively.

(C) DNA ploidy analyses immediately before and 28 h after differentiation induction using WT and the clock mutants (n = 10 cotyledons, mean). DNA ploidy distribution with or without VISUAL (top) and bar graphs of the fractions of 2C and 32C nuclei out of the total nuclei (bottom) are shown.

DISCUSSION

From the current actual-time-series single-cell analysis, we have here revealed that the oscillations of the clock genes are stopped in the reprogrammed cell state and are restarted during cell differentiation (Figures 3D and 3E). This result potentially explains the continuous phase resetting of *CCA1* expression in the root tip and the rephase of the circadian clock during the lateral

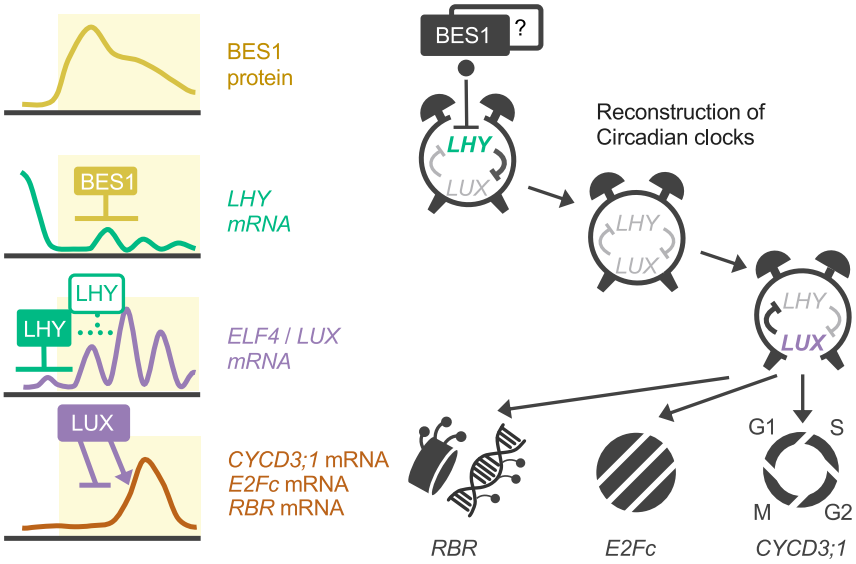

Figure 6. Dynamic changes in the *Arabidopsis* circadian clock prior to xylem cell differentiation

Our model proposes that BES1 represses *LHY* expression in reprogrammed cells to reconstruct the circadian clock, resulting in phase resetting and restarting of the clock with dynamic changes of clock gene expression. LUX in the reconstructed clock modulates key factors for cell-cycle progression, probably leading to cell differentiation.

root initiation (Fukuda et al., 2012; Voß et al., 2015). In addition, the expression profile of the clock genes was changed dynamically in the late stage of the reprogrammed cell state, prior to cell differentiation (Figure 4B). Plants have multiple circadian clocks, which show diverse properties with distinct expression profiles of clock genes and reside in different tissues (Endo et al., 2014; Inoue et al., 2018). Our results imply that the difference in expression profiles of clock genes and the features of tissue/organ-specific circadian clocks are established at an early stage of cell differentiation. Furthermore, our finding that the formation of circadian rhythms predates cell differentiation is consistent with a previous finding that the circadian clock regulates a large part of gene expressions, including key factors for cell differentiation (Michael et al., 2008).

In our ChIP-seq data, *CYCD3;1*, *RBR*, and *E2FC* were detected as LUX targets in the early differentiating cells (Figures 4C, 4D, and 5B). Previous reports have demonstrated that they all are involved in xylem differentiation (Kuwabara and Gruissem, 2014; Collins et al., 2015; Taylor-Teeples et al., 2015), supporting that they are highly potential targets of the circadian clock for cell differentiation. Proper expression levels of *E2FC* are significant for activating genes related to secondary cell wall biosynthesis (Taylor-Teeples et al., 2015). Given that the activity of E2FC for xylem differentiation is restricted by interaction with RBR (Taylor-Teeples et al., 2015), whose inhibitory activity is post-translationally controlled by CYCD3;1 (Kuwabara and Gruissem, 2014), LUX could contribute to fine-tuning both the expression and activity of E2FC under diel conditions for cell differentiation, although further analysis is needed to reveal how E2FC coordinates cell cycle with cell differentiation. In addition to *ELF4* and *LUX*, *TOC1* showed a high correlation coefficient with vascular stem cell markers (Figure 4B). TOC1 regulates cell division and DNA ploidy levels through direct regulation of CDC6, a DNA replication factor (Fung-Uceda et al., 2018). Our single-cell data showed that the timing of *CDC6* induction after differentiation induction was consistent with or slightly preceded that of *TOC1* (Figure S6), suggesting that TOC1 regulates expression of *CDC6* even in VISUAL. Given that *CDC6* was not detected as a direct target of LUX, TOC1 might also contribute to the regulation of cell cycle during vascular cell differentiation through a different pathway than LUX.

We demonstrated that the *bes1* and the clock mutants show similar defects in xylem cell differentiation in VISUAL (Figure 1B) and that BES1 directly binds to the promoter of *LHY* during the cell differentiation process (Figure 2B). In addition, suppression of *LHY* expression by BES1 was observed in our transient assay (Figure 2C) and the previous study (Yu et al., 2011). These findings suggest the significance of the BES1-*LHY* pathway for xylem cell differentiation, although further analyses would be needed to determine whether *LHY* suppression by BES1 in reprogrammed cells indeed triggers xylem differentiation. Since LHY represses expression of *ELF4* and *LUX* (Li et al., 2011; Nusinow et al., 2011), low expression levels of *LHY* probably caused by BES1 may lead to high expression levels of *ELF4* and *LUX*. This is consistent with a previous finding that clock genes that peaked in the morning, including *LHY*, are low, whereas the ones that peaked in the evening, including *ELF4* and *LUX*, are high in vasculature (Endo et al., 2014). Together, suppression of *LHY* by BES1 in reprogrammed cells may trigger reconstruction of circadian rhythms with dynamic changes of clock gene expression, including induction of *LUX*, and then LUX expressed in reprogrammed cells promotes xylem cell differentiation, probably through the direct regulation of key factors for cell-cycle progression (Figure 6).

In many multicellular organisms, the circadian clock controls cell division and cell differentiation (Brown, 2014). In plants, the current study shows that LUX has a potentially important role in co-regulating both cell-cycle progression and cell differentiation. These frameworks may be extended to animals that have independently acquired circadian clock systems during evolution (Hut and Beersma, 2011; Bhadra et al., 2017). Indeed, the mechanism for cell differentiation in plants and animals has functionally analogous features. These include (1) nuclear localization of non-phosphorylated forms of BES1 and β-catenin (Sharma et al., 2014), (2) inactivation by GSK3 kinase (Youn and Kim, 2015), (3) cell differentiation by CYCD/RB1 in animals and CYCD/RBR in plants (Desvoyes et al., 2014), and (4) inverse correlation between circadian clock oscillations and stemness (Figure 3E; Yagita et al., 2010). Convergent evolution of molecular mechanisms is also found in the innate immunity (Mermigka

et al., 2020), the developmental hourglass (Quint et al., 2012), the photoperiodicity, and the circadian clock system (Hut and Beersma, 2011; Bhadra et al., 2017) of plants and animals. Since the common mechanism beyond kingdoms is assumed to be deeply related to the essentials of its regulatory system, comparative studies of the mechanisms for cell differentiation in terms of the circadian clock will provide a new framework for understanding the basis of totipotency/pluripotency.

Overall, our study not only reveals a new role of the circadian clock in the regulation of cell differentiation but also provides a new pipeline to enable an actual time-series analysis of single-cell transcriptomics.

Limitations of the study

We showed that both BES1 and LHY regulate cell differentiation and that BES1 directly suppresses the expression of *LHY* in VISUAL. However, the extent to which the BES1-*LHY* pathway contributes to vascular cell differentiation is not yet demonstrated, and whether this pathway also regulates differentiation of other cell types remains to be elucidated.

Our time-series scRNA-seq data showed the cessation of circadian rhythms in reprogrammed cells and reconstruction of circadian rhythms prior to cell differentiation. It has to be noted that our data were derived from cells treated with the artificial VISUAL. The dynamic changes of the circadian clock system during cell differentiation in endogenous stem cells need to be examined.

STAR★METHODS

Detailed methods are provided in the online version of this paper and include the following:

- KEY RESOURCES TABLE
- RESOURCE AVAILABILITY
  - Lead contact
  - Materials availability
  - Data and code availability
- EXPERIMENTAL MODEL AND SUBJECT DETAILS
  - Arabidopsis thaliana
  - Nicotiana benthamiana
- METHOD DETAILS
  - GUS staining
  - DNA ploidy analyses
  - qRT-PCR
  - scRNA-seq and cpRNA-seq
  - Single cell isolation and cDNA library construction
  - Bulk treatment for NGS library construction
  - Wishbone – Seurat – PeakMatch pipeline
  - Overview of the PeakMatch algorithm
  - Performance comparison of PeakMatch algorithm
  - Plasmid construction
  - Western blotting
  - ChIP-qPCR and ChIP-seq
  - Transactivation assay
  - Detection of bioluminescence
- QUANTIFICATION AND STATISTICAL ANALYSIS
  - Measurement of xylem cell induction ratio
  - Measurement of stomatal index and root length

SUPPLEMENTAL INFORMATION

Supplemental information can be found online at https://doi.org/10.1016/j.celrep.2022.111059.

ACKNOWLEDGMENTS

We thank T. Koto, Y. Kanesaka, T. Kondo, and Y. Sando for technical assistance, R.M. Green, M. Ito, and N. Takahashi for useful feedback, J.A. Hejna for English proofreading, N. Mochizuki for the gift of *CAB2*::*GUS* seeds, T. Demura for the gift of *TDR*::*GUS* seeds, T. Nakano for the gift of *bes1-D* seeds, and N. Takahashi, T. Sugiyama, and M. Umeda for advising ploidy experiments. This work was supported by JST PRESTO Grant 888067 (to M.E.), by JSPS KAKENHI (grant numbers 20K21428, 18H02461, 19H05674, and 19H05670 (to M.E.), 19H05674, 19H04866, and 19K16170 (to A.K), 18K14732 and 20K15818 (to K.I.), and 17J08107 (to K.T.), by ISHIZUE 2017 of the Kyoto University Research Development Program, grants from the Yamada Science Foundation, Senri Life Science Foundation, Lotte Foundation, Daiichi Sankyo Foundation of Life Science, The Takeda Science Foundation, and the Nakajima Foundation, the Sekisui Chemical Grant Program, SEI Group CSR Foundation, Secom Science and Technology Foundation, Tokyo Kasei Chemical Promotion foundation (to M.E.), The Takeda Science Foundation, Senri Life Science Foundation, and The Mitsubishi Foundation (to A.K.), and by Grants-in-Aid for Scientific Research on Priority Area 25113005 (to T.A.). Sample preparation for RNA-seq and ChIP-seq was performed at the Medical Research Support Center, Graduate School of Medicine, Kyoto University.

AUTHOR CONTRIBUTIONS

K.T., K.I., K.B., H.S., A.K., and K.U. performed the gene expression analysis and phenotypic analysis. K.H. and K.T. performed the bioinformatic analysis. T.S., M.K., K.T., H.S., and M.E. performed the single-cell RNA-seq analysis. K.I. performed the ChIP assay. Y.K. assisted with VISUAL experiments. M.S. established BES1:BES1-GFP plants. K.T., K.I., and M.E. wrote the manuscript. M.E. directed and supervised the research with the support of T.A. and H.F.

DECLARATION OF INTERESTS

The authors declare no competing interests.

Received: June 9, 2021
Revised: April 1, 2022
Accepted: June 14, 2022
Published: July 12, 2022

REFERENCES

Aihara, K., Naramoto, S., Hara, M., and Mizoguchi, T. (2014). Increase in vascular pattern complexity caused by mutations in *LHY* and *CCA1* in *Arabidopsis thaliana* under continuous light. Plant Biotechnol. *31*, 43–47. https://doi.org/10.5511/plantbiotechnology.13.1015a.

Anders, S., and Huber, W. (2010). Differential expression analysis for sequence count data. Genome Biol. *11*, R106. https://doi.org/10.1186/gb-2010-11-10-r106.

Bhadra, U., Thakkar, N., Das, P., and Pal Bhadra, M. (2017). Evolution of circadian rhythms: from bacteria to human. Sleep Med. *35*, 49–61. https://doi.org/10.1016/j.sleep.2017.04.008.

Brown, S.A. (2014). Circadian clock-mediated control of stem cell division and differentiation: beyond night and day. Development *141*, 3105–3111. https://doi.org/10.1242/dev.104851.

Campbell, L., and Turner, S. (2017). Regulation of vascular cell division. J. Exp. Bot. *68*, 27–43. https://doi.org/10.1093/jxb/erw448.

Collins, C., Maruthi, N.M., and Jahn, C.E. (2015). CYCD3 D-type cyclins regulate cambial cell proliferation and secondary growth in Arabidopsis. J. Exp. Bot. *66*, 4595–4606. https://doi.org/10.1093/jxb/erv218.

de Jager, S.M., Scofield, S., Huntley, R.P., Robinson, A.S., den Boer, B.G.W., and Murray, J.A.H. (2009). Dissecting regulatory pathways of G_1/S control in *Arabidopsis*: common and distinct targets of CYCD3;1, E2Fa and E2Fc. Plant Mol. Biol. *71*, 345–365. https://doi.org/10.1007/s11103-009-9527-5.

De Veylder, L., Beeckman, T., and Inzé, D. (2007). The ins and outs of the plant cell cycle. Nat. Rev. Mol. Cell Biol. *8*, 655–665. https://doi.org/10.1038/nrm2227.

Desvoyes, B., de Mendoza, A., Ruiz-Trillo, I., and Gutierrez, C. (2014). Novel roles of plant RETINOBLASTOMA-RELATED (RBR) protein in cell proliferation and asymmetric cell division. J. Exp. Bot. *65*, 2657–2666. https://doi.org/10.1093/jxb/ert411.

Dewitte, W., Scofield, S., Alcasabas, A.A., Maughan, S.C., Menges, M., Braun, N., Collins, C., Nieuwland, J., Prinsen, E., Sundaresan, V., and Murray, J.A.H. (2007). *Arabidopsis* CYCD3 D-type cyclins link cell proliferation and endocycles and are rate-limiting for cytokinin responses. Proc. Natl. Acad. Sci. USA *104*, 14537–14542. https://doi.org/10.1073/pnas.0704166104.

Dierickx, P., Van Laake, L.W., and Geijsen, N. (2018). Circadian clocks: from stem cells to tissue homeostasis and regeneration. EMBO Rep. *19*, 18–28. https://doi.org/10.15252/embr.201745130.

Endo, M., Shimizu, H., Nohales, M.A., Araki, T., and Kay, S.A. (2014). Tissue-specific clocks in *Arabidopsis* show asymmetric coupling. Nature *515*, 419–422. https://doi.org/10.1038/nature13919.

Ezer, D., Jung, J.H., Lan, H., Biswas, S., Gregoire, L., Box, M.S., Charoensawan, V., Cortijo, S., Lai, X., Stöckle, D., et al. (2017). The evening complex coordinates environmental and endogenous signals in *Arabidopsis*. Nat. Plants *3*, 17087. https://doi.org/10.1038/nplants.2017.87.

Fukuda, H., Ukai, K., and Oyama, T. (2012). Self-arrangement of cellular circadian rhythms through phase-resetting in plant roots. Phys. Rev. E Stat. Nonlin. Soft Matter Phys. *86*, 041917. https://doi.org/10.1103/PhysRevE.86.041917.

Fung-Uceda, J., Lee, K., Seo, P.J., Polyn, S., De Veylder, L., and Mas, P. (2018). The circadian clock sets the time of DNA replication licensing to regulate growth in Arabidopsis. Dev. Cell *45*, 101–113.e4. https://doi.org/10.1016/j.devcel.2018.02.022.

Golden, S.S., Ishiura, M., Johnson, C.H., and Kondo, T. (1997). Cyanobacterial circadian rhythms. Annu. Rev. Plant Physiol. Plant Mol. Biol. *48*, 327–354. https://doi.org/10.1146/annurev.arplant.48.1.327.

Harashima, H., and Schnittger, A. (2010). The integration of cell division, growth and differentiation. Curr. Opin. Plant Biol. *13*, 66–74. https://doi.org/10.1016/j.pbi.2009.11.001.

Helfer, A., Nusinow, D.A., Chow, B.Y., Gehrke, A.R., Bulyk, M.L., and Kay, S.A. (2011). *LUX ARRHYTHMO* encodes a nighttime repressor of circadian gene expression in the *Arabidopsis* core clock. Curr. Biol. *21*, 126–133. https://doi.org/10.1016/j.cub.2010.12.021.

Hut, R.A., and Beersma, D.G.M. (2011). Evolution of time-keeping mechanisms: early emergence and adaptation to photoperiod. Philos. Trans. R. Soc. Lond. B Biol. Sci. *366*, 2141–2154. https://doi.org/10.1098/rstb.2010.0409.

Inoue, K., Araki, T., and Endo, M. (2018). Oscillator networks with tissue-specific circadian clocks in plants. Semin. Cell Dev. Biol. *83*, 78–85. https://doi.org/10.1016/j.semcdb.2017.09.002.

Islam, S., Zeisel, A., Joost, S., La Manno, G., Zajac, P., Kasper, M., Lönnerberg, P., and Linnarsson, S. (2014). Quantitative single-cell RNA-seq with unique molecular identifiers. Nat. Methods *11*, 163–166. https://doi.org/10.1038/nmeth.2772.

Kang, C.Y., Lian, H.L., Wang, F.F., Huang, J.R., and Yang, H.Q. (2009). Cryptochromes, phytochromes, and COP1 regulate light-controlled stomatal development in *Arabidopsis*. Plant Cell *21*, 2624–2641. https://doi.org/10.1105/tpc.109.069765.

Kim, D., Langmead, B., and Salzberg, S.L. (2015). HISAT: a fast spliced aligner with low memory requirements. Nat. Methods *12*, 357–360. https://doi.org/10.1038/nmeth.3317.

Kondo, Y., Ito, T., Nakagami, H., Hirakawa, Y., Saito, M., Tamaki, T., Shirasu, K., and Fukuda, H. (2014). Plant GSK3 proteins regulate xylem cell differentiation downstream of TDIF-TDR signalling. Nat. Commun. *5*, 3504. https://doi.org/10.1038/ncomms4504.

Kondo, Y., Nurani, A.M., Saito, C., Ichihashi, Y., Saito, M., Yamazaki, K., Mitsuda, N., Ohme-Takagi, M., and Fukuda, H. (2016). Vascular cell induction culture system using Arabidopsis leaves (VISUAL) reveals the sequential differentiation of sieve element-like cells. Plant Cell *28*, 1250–1262. https://doi.org/10.1105/tpc.16.00027.

Kowalska, E., Moriggi, E., Bauer, C., Dibner, C., and Brown, S.A. (2010). The circadian clock starts ticking at a developmentally early stage. J. Biol. Rhythms *25*, 442–449. https://doi.org/10.1177/0748730410385281.

Kubo, M., Nishiyama, T., Tamada, Y., Sano, R., Ishikawa, M., Murata, T., Imai, A., Lang, D., Demura, T., Reski, R., and Hasebe, M. (2019). Single-cell transcriptome analysis of Physcomitrella leaf cells during reprogramming using microcapillary manipulation. Nucleic Acids Res. *47*, 4539–4553. https://doi.org/10.1093/nar/gkz181.

Kuwabara, A., and Gruissem, W. (2014). *Arabidopsis* RETINOBLASTOMA-RELATED and Polycomb group proteins: cooperation during plant cell differentiation and development. J. Exp. Bot. *65*, 2667–2676. https://doi.org/10.1093/jxb/eru069.

Langmead, B., Trapnell, C., Pop, M., and Salzberg, S.L. (2009). Ultrafast and memory-efficient alignment of short DNA sequences to the human genome. Genome Biol. *10*, R25. https://doi.org/10.1186/gb-2009-10-3-r25.

Li, L., Yu, X., Thompson, A., Guo, M., Yoshida, S., Asami, T., Chory, J., and Yin, Y. (2009). *Arabidopsis* MYB30 is a direct target of BES1 and cooperates with BES1 to regulate brassinosteroid-induced gene expression. Plant J. *58*, 275–286. https://doi.org/10.1111/j.1365-313X.2008.03778.x.

Li, G., Siddiqui, H., Teng, Y., Lin, R., Wan, X.y., Li, J., Lau, O.S., Ouyang, X., Dai, M., Wan, J., et al. (2011). Coordinated transcriptional regulation underlying the circadian clock in *Arabidopsis*. Nat. Cell Biol. *13*, 616–622. https://doi.org/10.1038/ncb2219.

Li, Q.F., Lu, J., Yu, J.W., Zhang, C.Q., He, J.X., and Liu, Q.Q. (2018). The brassinosteroid-regulated transcription factors BZR1/BES1 function as a coordinator in multisignal-regulated plant growth. Biochim. Biophys. Acta Gene Regul. Mech. *1861*, 561–571. https://doi.org/10.1016/j.bbagrm.2018.04.003.

Malucelli, F., Ottmann, T., and Pretolani, D. (1993). Efficient labelling algorithms for the maximum noncrossing matching problem. Discrete Appl. Math. *47*, 175–179. https://doi.org/10.1007/978-3-642-77489-8_30.

Mermigka, G., Amprazi, M., Mentzelopoulou, A., Amartolou, A., and Sarris, P.F. (2020). Plant and animal innate immunity complexes: fighting different enemies with similar weapons. Trends Plant Sci. *25*, 80–91. https://doi.org/10.1016/j.tplants.2019.09.008.

Michael, T.P., Mockler, T.C., Breton, G., McEntee, C., Byer, A., Trout, J.D., Hazen, S.P., Shen, R., Priest, H.D., Sullivan, C.M., et al. (2008). Network discovery pipeline elucidates conserved time-of-day–specific cis-regulatory modules. PLoS Genet. *4*, e14. https://doi.org/10.1371/journal.pgen.0040014.

Nakagawa, T., Kurose, T., Hino, T., Tanaka, K., Kawamukai, M., Niwa, Y., Toyooka, K., Matsuoka, K., Jinbo, T., and Kimura, T. (2007). Development of series of gateway binary vectors, pGWBs, for realizing efficient construction of fusion genes for plant transformation. J. Biosci. Bioeng. *104*, 34–41. https://doi.org/10.1263/jbb.104.34.

Nelms, B., and Walbot, V. (2019). Defining the developmental program leading to meiosis in maize. Science *364*, 52–56. https://doi.org/10.1126/science.aav6428.

Nishimura, T., Yokota, E., Wada, T., Shimmen, T., and Okada, K. (2003). An *Arabidopsis ACT2* dominant-negative mutation, which disturbs F-actin polymerization, reveals its distinctive function in root development. Plant Cell Physiol. *44*, 1131–1140. https://doi.org/10.1093/pcp/pcg158.

Niwa, Y., Ito, S., Nakamichi, N., Mizoguchi, T., Niinuma, K., Yamashino, T., and Mizuno, T. (2007). Genetic linkages of the circadian clock-associated genes, *TOC1, CCA1* and *LHY*, in the photoperiodic control of flowering time in *Arabidopsis thaliana*. Plant Cell Physiol. *48*, 925–937. https://doi.org/10.1093/pcp/pcm067.

Nusinow, D.A., Helfer, A., Hamilton, E.E., King, J.J., Imaizumi, T., Schultz, T.F., Farré, E.M., and Kay, S.A. (2011). The ELF4-ELF3-LUX complex links the circadian clock to diurnal control of hypocotyl growth. Nature *475*, 398–402. https://doi.org/10.1038/nature10182.

Paulose, J.K., Rucker, E.B., and Cassone, V.M. (2012). Toward the beginning of time: circadian rhythms in metabolism precede rhythms in clock gene expression in mouse embryonic stem cells. PLoS One *7*, e49555. https://doi.org/10.1371/journal.pone.0049555.

Quint, M., Drost, H.G., Gabel, A., Ullrich, K.K., Bönn, M., and Grosse, I. (2012). A transcriptomic hourglass in plant embryogenesis. Nature *490*, 98–101. https://doi.org/10.1038/nature11394.

Ryu, K.H., Huang, L., Kang, H.M., and Schiefelbein, J. (2019). Single-cell RNA sequencing resolves molecular relationships among individual plant cells. Plant Physiol. *179*, 1444–1456. https://doi.org/10.1104/pp.18.01482pp.18.01482.

Saito, M., Kondo, Y., and Fukuda, H. (2018). BES1 and BZR1 redundantly promote phloem and xylem differentiation. Plant Cell Physiol. *59*, 590–600. https://doi.org/10.1093/pcp/pcy012.

Satija, R., Farrell, J.A., Gennert, D., Schier, A.F., and Regev, A. (2015). Spatial reconstruction of single-cell gene expression data. Nat. Biotechnol. *33*, 495–502. https://doi.org/10.1038/nbt.3192.

Schaffer, R., Ramsay, N., Samach, A., Corden, S., Putterill, J., Carre, I.A., and Coupland, G. (1998). The late elongated hypocotyl mutation of Arabidopsis disrupts circadian rhythms and the photoperiodic control of flowering. Cell *93*, 1219–1229. https://doi.org/10.1016/S0092-8674(00)81465-8.

Setty, M., Tadmor, M.D., Reich-Zeliger, S., Angel, O., Salame, T.M., Kathail, P., Choi, K., Bendall, S., Friedman, N., and Pe'er, D. (2016). Wishbone identifies bifurcating developmental trajectories from single-cell data. Nat. Biotechnol. *34*, 637–645. https://doi.org/10.1038/nbt.3569.

Sharma, M., Pandey, A., and Pandey, G.K. (2014). β-catenin in plants and animals: common players but different pathwaysî^2-catenin in plants and animals: common players but different pathways. Front. Plant Sci. *5*, 143. https://doi.org/10.3389/fpls.2014.00143.

Shimada, T.L., Shimada, T., and Hara-Nishimura, I. (2010). A rapid and non-destructive screenable marker, FAST, for identifying transformed seeds of *Arabidopsis thaliana*. Plant J. *61*, 519–528. https://doi.org/10.1111/j.1365-313X.2009.04060.x.

Shulse, C.N., Cole, B.J., Ciobanu, D., Lin, J., Yoshinaga, Y., Gouran, M., Turco, G.M., Zhu, Y., O'Malley, R.C., Brady, S.M., and Dickel, D.E. (2019). High-throughput single-cell transcriptome profiling of plant cell types. Cell Rep. *27*, 2241–2247.e4. https://doi.org/10.1016/j.celrep.2019.04.054.

Sun, N., Yu, X., Li, F., Liu, D., Suo, S., Chen, W., Chen, S., Song, L., Green, C.D., McDermott, J., et al. (2017). Inference of differentiation time for single cell transcriptomes using cell population reference data. Nat. Commun. *8*, 1856. https://doi.org/10.1038/s41467-017-01860-2.

Taylor-Teeples, M., Lin, L., de Lucas, M., Turco, G., Toal, T.W., Gaudinier, A., Young, N.F., Trabucco, G.M., Veling, M.T., Lamothe, R., et al. (2015). An *Arabidopsis* gene regulatory network for secondary cell wall synthesis. Nature *517*, 571–575. https://doi.org/10.1038/nature14099.

Tsuchiya, Y., Umemura, Y., and Yagita, K. (2020). Circadian clock and cancer: from a viewpoint of cellular differentiation. Int. J. Urol. *27*, 518–524. https://doi.org/10.1111/iju.14231.

Voß, U., Wilson, M.H., Kenobi, K., Gould, P.D., Robertson, F.C., Peer, W.A., Lucas, M., Swarup, K., Casimiro, I., Holman, T.J., et al. (2015). The circadian clock rephases during lateral root organ initiation in *Arabidopsis thaliana*. Nat. Commun. *6*, 7641. https://doi.org/10.1038/ncomms8641.

Weger, M., Diotel, N., Dorsemans, A.C., Dickmeis, T., and Weger, B.D. (2017). Stem cells and the circadian clock. Dev. Biol. *431*, 111–123. https://doi.org/10.1016/j.ydbio.2017.09.012.

Yagita, K., Horie, K., Koinuma, S., Nakamura, W., Yamanaka, I., Urasaki, A., Shigeyoshi, Y., Kawakami, K., Shimada, S., Takeda, J., and Uchiyama, Y. (2010). Development of the circadian oscillator during differentiation of mouse embryonic stem cells in vitro. Proc. Natl. Acad. Sci. USA *107*, 3846–3851. https://doi.org/10.1073/pnas.0913256107.

Yamaguchi, M., Mitsuda, N., Ohtani, M., Ohme-Takagi, M., Kato, K., and Demura, T. (2011). VASCULAR-RELATED NAC-DOMAIN7 directly regulates the expression of a broad range of genes for xylem vessel formation. Plant J. *66*, 579–590. https://doi.org/10.1111/j.1365-313X.2011.04514.x.

Yamaguchi, N., Winter, C.M., Wu, M.F., Kwon, C.S., William, D.A., and Wagner, D. (2014). PROTOCOLS: chromatin immunoprecipitation from *Arabidopsis* tissues. Arabidopsis Book *12*, e0170. https://doi.org/10.1199/tab.0170.

Yamazaki, K., Kondo, Y., Kojima, M., Takebayashi, Y., Sakakibara, H., and Fukuda, H. (2018). Suppression of DELLA signaling induces procambial cell formation in culture. Plant J. *94*, 48–59. https://doi.org/10.1111/tpj.13840.

Yin, Y., Wang, Z.Y., Mora-Garcia, S., Li, J., Yoshida, S., Asami, T., and Chory, J. (2002). BES1 accumulates in the nucleus in response to brassinosteroids to regulate gene expression and promote stem elongation. Cell *109*, 181–191. https://doi.org/10.1016/s0092-8674(02)00721-3.

Youn, J.H., and Kim, T.W. (2015). Functional insights of plant GSK3-like kinases: multi-taskers in diverse cellular signal transduction pathways. Mol. Plant *8*, 552–565. https://doi.org/10.1016/j.molp.2014.12.006.

Yu, X., Li, L., Zola, J., Aluru, M., Ye, H., Foudree, A., Guo, H., Anderson, S., Aluru, S., Liu, P., et al. (2011). A brassinosteroid transcriptional network revealed by genome-wide identification of BESI target genes in *Arabidopsis thaliana*. Plant J. *65*, 634–646. https://doi.org/10.1111/j.1365-313X.2010.04449.x.

Yu, X., Rollins, D., Ruhn, K.A., Stubblefield, J.J., Green, C.B., Kashiwada, M., Rothman, P.B., Takahashi, J.S., and Hooper, L.V. (2013). TH17 cell differentiation is regulated by the circadian clock. Science *342*, 727–730. https://doi.org/10.1126/science.1243884.

Zhang, Y., Liu, T., Meyer, C.A., Eeckhoute, J., Johnson, D.S., Bernstein, B.E., Nusbaum, C., Myers, R.M., Brown, M., Li, W., and Liu, X.S. (2008). Model-based analysis of ChIP-seq (MACS). Genome Biol. *9*, R137. https://doi.org/10.1186/gb-2008-9-9-r137.

STAR★METHODS

KEY RESOURCES TABLE

REAGENT or RESOURCE	SOURCE	IDENTIFIER
Antibodies		
Rabbit polyclonal anti-GFP	MBL	Cat# 598, RRID:AB_591819
Bacterial and virus strains		
Agrobacterium tumefaciens		GV3101 pMP90
Chemicals, peptides, and recombinant proteins		
Bikinin	Merck	SML0094-25MG
2,4-dichlorophenoxyacetic acid (2,4-D)	FUJIFILM Wako Pure Chemical Corporation	040–18532
6-Furfurylaminopurine (Kinetin)	FUJIFILM Wako Pure Chemical Corporation	116–00333
Critical commercial assays		
TruSeq ChIP Sample Preparation Kit	Illumina	IP-202-1012
Dual-Luciferase Reporter Assay System	Promega	E1910
Deposited data		
Data for scRNA-seq, cpRNA-seq, and ChIP-seq	NCBI	SRA: PRJNA551314
Experimental models: Organisms/strains		
Nicothiana benthamiana		N/A
Arabidopsis thaliana ecotype Columbia		N/A
LUX::*LUX-GFP/lux-4*	Ezer et al. (2017)	N/A
CAB2::*LUC*, *lux nox*	Helfer et al. (2011)	N/A
cca1-1 lhy-11 toc1-2	Niwa et al. (2007)	N/A
IRX3::*GUS*	This paper	N/A
35S::*LHY*	This paper	N/A
BES1::*BES1-GFP*	This paper	N/A
LHY::*LUC*	This paper	N/A
Oligonucleotides		
See Table S5	This paper	N/A
Recombinant DNA		
Plasmid: IRX3::GUS	This paper	N/A
Plasmid: 35S::LHY	This paper	N/A
Plasmid: BES1::BES1-GFP	This paper	N/A
Plasmid: LHY::LUC	This paper	N/A
Plasmid: 35S::bes1-D	This paper	N/A
Plasmid: 35S::RLUC	This paper	N/A
Software and algorithms		
PeakMatch	This paper	https://github.com/endo-lab/PeakMatch
Wishbone (v0.4.2)	Setty et al. (2016)	https://github.com/ManuSetty/wishbone
Seurat (v1.2.1)	Satija et al. (2015)	https://satijalab.org/seurat/
Bowtie	Langmead et al. (2009)	http://bowtie-bio.sourceforge.net/index.shtml
DEseq (v1.34.1)	Anders and Huber (2010)	http://bioconductor.org/packages/release/bioc/html/DESeq.html; v.1.34.1
iCpSc	Sun et al. (2017)	https://www.picb.ac.cn/hanlab/iCpSc.html
HISAT2 (v2.1.0)	Kim et al. (2015)	http://daehwankimlab.github.io/hisat2/
MACS2 (v2.1.2)	Zhang et al. (2008)	https://pypi.org/project/MACS2/

RESOURCE AVAILABILITY

Lead contact

Further information and requests for resources and reagents should be directed to and will be fulfilled by the lead contact, Motomu Endo (endo@bs.naist.jp).

Materials availability

Plasmids and plant materials generated in this research are all available on request to the lead contact, Motomu Endo (endo@bs.naist.jp).

Data and code availability

- All deep sequencing data have been deposited in NCBI SRA: PRJNA551314 and are publicly available as of the date of publication.
- All code used to generate the figures is available online at https://github.com/endo-lab/PeakMatch.
- Any additional information required to reanalyze the data reported in this paper is available from the lead contact upon request.

EXPERIMENTAL MODEL AND SUBJECT DETAILS

Arabidopsis thaliana

All the wild type and transgenic lines used here were *Arabidopsis thaliana* ecotype Columbia-0 (Col-0). Seeds were surface-sterilized and sown on 0.8% agar plates containing Murashige and Skoog medium with 0.5% sucrose or liquid media as described previously (Kondo et al., 2016). Plants were grown under 12L/12D (12 h light and 12 h dark, 84 μmol m^{-2} s^{-1}) conditions at 22°C. For induction of ectopic vascular cell differentiation, plants were entrained by 12L/12D conditions for 7 days, although the original protocols (Kondo et al., 2016) called for growth of plants under continuous light (LL) conditions. Bikinin, 2,4-dichlorophenoxyacetic acid (2,4-D), and kinetin were added to the 8-day-old plants at ZT0. *cca1-1 lhy-11 toc1-2* was provided by Takafumi Yamashino (Niwa et al., 2007) (Nagoya University), *lux nox* and its parental *CAB2*::*LUC* were provided by Dmitri A. Nusinow (Helfer et al., 2011) (Donald Danforth Plant Science Center), *LUX*::*LUX-GFP/lux-4* was provided by Philip A. Wigge (Ezer et al., 2017) (University of Cambridge).

Nicotiana benthamiana

For transactivation assays, *Nicotiana benthamiana* seeds were sown directly on soil and grown under 12L/12D (12 h light and 12 h dark, ~120 μmol m^{-2} s^{-1}) conditions at 25°C.

METHOD DETAILS

GUS staining

Plants were fixed in 90%(v/v) acetone for 15 min on ice, vacuum-infiltrated and incubated at 37°C for 2 h (overnight for *IRX3*::*GUS*) in the GUS assay solution containing 100 mM sodium phosphate buffer (pH 7.2), 1 mM potassium-ferrocyanide (5 mM for *TDR*::*GUS*), 1 mM potassium-ferricyanide (5 mM for *TDR*::*GUS*), 0.1%(v/v) Triton X-100 and 0.5 mg mL^{-1} 5-bromo-4-chloro-3-indolyl-β-D-glucuronic acid (X-Gluc). Chlorophylls in the tissue were removed by incubation in 70%(v/v) ethanol.

DNA ploidy analyses

Plants immediately before and 28 h after differentiation induction in VISUAL were used. Cotyledons were chopped using a razor blade in 0.5 mL of nuclei-extraction buffer (solution A of the Cystain UV precise P; Partec). After filtration through a 30-μm mesh, 2 mL of the staining solution containing DAPI (solution B of the kit) was added. Ploidy levels were measured using a ploidy analyzer PA (Partec). The lowest peak of WT was assumed to represent 2C nuclei (C is the haploid DNA content).

qRT-PCR

Total RNA was extracted using an RNeasy Plant Mini Kit (QIAGEN) and reverse-transcribed using a Transcriptor First Strand cDNA Synthesis Kit (Roche) according to the manufacturer's instructions.

Real-time gene expression was analyzed with a CFX96 Real-Time PCR Detection System (Bio-Rad). *UBQ14* was used as an internal control for VISUAL experiments (Kondo et al., 2016). Specific sequences for each primer pair were listed in Table S5.

The following thermal cycling profile was used, CAB3, 95°C for 10 s, ~40 cycles of 95°C for 10 s, 62°C for 15 s, and 72°C for 15 s; IRX3, 95°C for 60 s, ~40 cycles of 95°C for 10 s, 64.5°C for 15 s, and 72°C for 10 s;

ANT, VND7, and HAM2, 95°C for 30 s, ~40 cycles of 95°C for 5 s and 60°C for 30 s; and

TDR, LHY, CYCD3;1, E2FC, and UBQ14, 95°C for 60 s, ~40 cycles of 95°C for 10 s, 60°C for 15 s, and 72°C for 15 s.

Each sample was run in technical triplicate to reduce experimental errors. Error bars, representing standard errors, were calculated from the results of biological triplicates.

scRNA-seq and cpRNA-seq

For scRNA-seq, the process closely followed the method as described previously (Kubo et al., 2019). A cotyledon before and after treatment with VISUAL for the indicated time periods was placed adaxial side down on a glass slide, and fixed with an adhesive tape, e.g., cellophane tape. Then the center of cotyledon was cut using a razor blade, and with the aid of a microscope, the contents of a single cell were collected using a glass capillary. Samples were subjected to UMI-tagged sequencing using a NextSeq 500 system (Illumina). Detailed methods are described below. For cpRNA-seq, total RNA was extracted using an RNeasy Plant Mini Kit and subjected to UMI-tagged sequencing, as for scRNA-seq, except that 10 cycles of the PCR amplification step were required. Sequence reads were mapped against to the TAIR10 *Arabidopsis* cDNA sequence by Bowtie (Langmead et al., 2009) with the parameter "-a –best –strata". Gene expression level was quantified by counting the absolute number of UMIs mapped to each gene. scRNA-seq data was normalized together with cpRNA-seq using the R/Bioconductor DESeq (Anders and Huber, 2010) package (http://bioconductor.org/packages/release/bioc/html/DESeq.html; v.1.34.1).

Single cell isolation and cDNA library construction

A set of oil hydraulic micromanipulators (MMO-220A and MMO-202ND; Narishige) and motor-driven manipulators MM-89 (Narishige) were equipped onto an inverted fluorescent microscope IX-70 (Olympus). The 1.0-mm capillary holder was connected to a microinjector (CellTram vario) via a silicone tube filled with mineral oil (Sigma-Aldrich), which was in turn attached to the MMO-220A micromanipulator. The parameters of the 1.0-mm glass capillaries were as follows: inner diameter: 20 μm, pipette form: straight, beveled angle of tip: 40°, and pipette length: 55 mm (BioMedical Instruments). The bottom of the glass capillary contained a small amount of cell content extraction mix2 comprising 13% of 10×PCR buffer II (Thermo Fisher Scientific), 7.8% of 25 mM $MgCl_2$, 6.5% of 0.1M DTT, 2.6% of RNasin Plus RNase inhibitor (Promega), and 2.6% of 2.5 mM dNTPs (TaKaRa). The attached microcapillary was gently filled with mineral oil under a microscope using the CellTram vario. After adjusting the tip position of the glass capillary to the center of the observation field, a dish containing an excised cotyledon was set on the microscope and the tip of the capillary was used to extract the cell contents from the target cell. The cell contents were immediately transferred into a 0.2-mL PCR tube containing 1.25 μL of 0.05 μM RT oligos and 2.35 μL of cell content extraction mix1 comprising 0.45 μL of 10×PCR buffer II, 0.27 μL of 25 mM $MgCl_2$, 0.225 μL of 0.1 M DTT, 0.09 μL of RNasin Plus RNase inhibitor, 0.09 μL of 2.5 mM dNTPs, and 0.1 μL of 20,000-fold diluted ERCC RNA spike-in mix (Thermo Fisher Scientific). After a brief centrifugation, the samples were primed with an incubation on a thermal cycler at 70°C for 90 s, 35°C for 15 s, and cooled to 4°C. The RT oligos used in this work were described previously (Kubo et al., 2019).

For the reverse transcription, a 0.9 μL of RT mix comprising 0.33 μL of SuperScript IV reverse transcriptase (Thermo Fisher Scientific), 0.05 μL of RNasin plus RNase Inhibitor, and 0.07 μL of T4 gene 32 protein (New England Biolabs) was added to each primed RNA solution, and incubated at 50°C for 30 min, 70°C for 10 min, and cooled to 4°C. To digest the excess RT oligos, the samples were mixed with 0.8 μL of nuclease-free water (QIAGEN), 0.1 μL of 10×exonuclease I buffer, and 0.1 μL of 20 U/μL exonuclease I (New England Biolabs), and incubated on a thermal cycler using the following conditions: 4°C for 30 s, 37°C for 30 min, 80°C for 20 min with lid heating at 90°C, and cooled to 4°C. The poly(dA) mix for poly(dA) tailing with RNaseH was as follows: 4.44 μL of nuclease-free water, 0.6 μL of 10×PCR buffer II, 0.36 μL of 25 mM $MgCl_2$, 0.18 μL of 100 mM dATP (New England Biolabs), 0.3 μL of 15 U/μL terminal deoxynucleotidyl transferase (Thermo Fisher Scientific), and 0.12 μL of 5 U/μL RNaseH (New England Biolabs). Six-μL of the poly(dA) mix was added after the exonuclease I treatment, and the mixture were incubated on a thermal cycler using the following conditions: 4°C for 30 s, 37°C for 1.5 min, 70°C for 10 min with lid heating at 80°C, and cooled to 4°C. For the second-strand synthesis, the following PCR mix1 was prepared: 50.68 μL of nuclease-free water, 15.2 μL of 5×Q5 reaction buffer with $MgCl_2$ (New England Biolabs), 7.6 μL of 2.5 mM dNTPs, 0.76 μL of 100 μM NUP3 primer listed in Tables S5, and 1.76 μL of Q5 Hot Start High-Fidelity DNA polymerase (2 U/μL) (New England Biolabs). 76 μL of PCR mix1 was added after the poly(dA) tailing, and then the mixtures were divided into 21-μL aliquots which were transferred into four new 0.2-mL PCR tubes and incubated on a thermal cycler using the following conditions: 95°C for 3 min, 98°C for 20 s, 50°C for 2 min, 72°C for 10 min, and cooled to 4°C. For the cDNA amplification, the following PCR mix2 was prepared: 12.73 μL of nuclease-free water, 3.8 μL of 5×Q5 reaction buffer with $MgCl_2$, 1.9 μL of 2.5 mM dNTPs, 0.19 μL of 100 μM BTEP7v2 primer listed in Tables S5, and 0.38 μL of Q5 Hot Start High-Fidelity DNA polymerase. 19-μL of PCR mix2 was added to each tube after the second-strand synthesis, pipetted to mix and briefly centrifuged. The tubes were incubated on a thermal cycler using the following conditions: an initial denaturation at 95°C for 3 min; followed by 22 cycles of 98°C for 10 s, 60°C for 30 s, and 72°C for 6 min, which extended by 6 s at 72°C in each cycle; and stored at 4°C. After the PCR amplification, the cDNA libraries were purified using a PureLink PCR purification kit with Binding Buffer High-Cutoff (Thermo Fisher Scientific), according to the manufacturer's instructions. To check availability of each sample, the quantity and quality of the cDNA libraries were measured using a Bioanalyzer 2100 with a High Sensitivity DNA kit (Agilent Technologies). Each cDNA library solution was placed in a 1.5-mL DNA Lo-bind tube (Eppendorf) and adjusted to a volume of 35 μL with elution buffer (EB) comprising 10 mM Tris–HCl (pH 8.0). To remove the byproducts in the cDNA libraries, a 0.55×volume of SPRIselect beads (Beckman Coulter) were added to each cDNA library solution, which adhered the appropriately sized cDNAs. The tubes were placed on a MagnaStand (Nippon Genetics) for 3 min, and the beads collected at the bottom of the tube. The supernatants were gently removed by aspiration, after which the beads were rinsed twice with 80% ethanol. After air-drying for 10 min, the beads were re-suspended in 50 μL of EB, and then left to stand on the Magna stand for 3 min. The resulting supernatants were recovered into new 1.5-mL DNA Lo-bind tubes. Purification with the SPRIselect beads was carried out at least three times. The quantity and quality of the purified cDNA libraries were

measured using a Bioanalyzer 2100 with a High Sensitivity DNA kit, and the purified cDNA libraries were stored at −30°C until required.

Bulk treatment for NGS library construction

In order to fragment the cDNAs to construct the NGS libraries, 2.5 nmol each of four or five purified cDNA libraries were combined, and the volume of the resulting solution was increased to 75 μL with EB. The mixtures were transferred into microTUBE AFA Fiber Pre-Snap-Cap tubes (Covaris) and care was taken to prevent any air bubbles. cDNA shearing with a target peak of ∼400 bp was carried out using an acoustic solubilizer, Covaris S220 (Covaris), under the following conditions; bath temperature: 4–8°C, degassing mode: continuous, power mode: frequency sweeping, duty cycle: 10%, intensity: 3, cycles/burst: 200, and time: 90 s. After this treatment, the fragmented cDNAs were transferred to new 1.5-mL DNA Lo-bind tubes and purified with a MinElute PCR purification kit (QIAGEN). The quality of the fragmented cDNA was measured using a Bioanalyzer 2100 with a High Sensitivity DNA kit. To recover the fragmented cDNAs tagged with biotin, 20 μL of streptavidin-linked beads, Dynabeads MyOne Streptavidin C1 (Thermo Fisher Scientific), were rinsed twice with 2×BWT buffer comprising 10 mM Tris–HCl (pH 7.5), 1 mM EDTA, 2 M NaCl, and 0.02% Tween-20, then suspended in an equal volume of the fragmented cDNA solution. The solutions were left to stand for 10 min to bind the biotinylated cDNA fragments, then placed on a MagnaStand for 30 s. The supernatants were discarded and the beads were rinsed three times with 1× BWT buffer and re-suspended in 25 μL of EBT buffer containing 10mM Tris–HCl (pH 8.5) and 0.02% Tween-20. For the end repair, a 25-μL mixture containing 5 μL of 10×NEBnext End Repair Reaction Buffer (New England Biolabs) and 2.5 μL of NEBnext End Repair Enzyme Mix (New England Biolabs) was added to the mixture of beads and cDNA fragments. The solution was mixed by gently pipetting and centrifuging briefly, and then incubated at room temperature with shaking at 400 rpm for 30 min. The tubes were stood on a MagnaStand for 30 s and the supernatants were discarded. The beads were then rinsed twice with 1× BWT buffer while on the MagnaStand, after which the stand was removed to enable the beads to be re-suspended in 21 μL of EBT buffer. For the dA-tailing, a commercial reagent kit, NEBNextdA-tailing Module (New England Biolabs), was utilized. A 4-μL aliquot of a mixture containing 2.5 μL of 10×NEBnext dA-Tailing reaction buffer (New England Biolabs) and 1.5 μL of Klenow Fragment (3-> 5exo-) (New England Biolabs) was added to the solution of beads with end-repaired cDNA fragments. The mixtures were pipetted gently to mix and briefly centrifuged before being incubated at 37°C with shaking at 400 rpm for 30 min. To remove the reaction mix, the tubes were stood on a MagnaStand for 30 s and the supernatants were discarded. The beads were rinsed twice with 1×BWT buffer and re-suspended in 25 μL of EBT buffer. To ligate the adapters to the cDNA, a 25-μL mixture containing 5 μL of 10×T4 DNA ligase buffer (New England Biolabs), 1.5 μL of 100 μM RP1 adaptor v2 listed in Tables S5, and 5 μL of 400U/μL T4 DNA ligase (New England Biolabs) was added to the solution containing the beads and dA-tailed cDNA fragments. The solutions were mixed by gently pipetting then centrifuged briefly, after which they were incubated at 20°C with shaking at 400 rpm for 20 min. A 5-μL aliquot of 1U/μL USER Enzyme (New England Biolabs) was added to each tube, pipetted gently to mix, then incubated at 37°C with shaking at 400 rpm for 60 min. To remove the reaction mix, the tubes were stood on a Magna stand for 30 s and the supernatants were discarded. The beads were rinsed twice with 1×BWT buffer and re-suspended in 25 μL of EBT buffer. To fill the 5′-overhang in the cDNA, a 5-μL mixture containing 3 μL of 10×NEB buffer 2 (New England Biolabs), 1 μL of 2.5 mM dNTPs (TaKaRa), and 1 μL of 10 U/μL DNA pol I (New England Biolabs) was added to the solution of adaptor-ligated cDNA fragments and beads. After pipetting gently to mix and centrifuging briefly, the tubes were incubated at 37°C with shaking at 400 rpm for 30 min. To remove the reaction mix, the tubes were stood on a MagnaStand for 30 s and the supernatants were discarded. The beads were then rinsed twice with 1×BWT buffer and re-suspended in 25 μL of EBT buffer. For the library enrichment, the following PCR mix3 was prepared: 50 μL of nuclease-free water (QIAGEN), 20 μL of 5×KAPA HiFi reaction buffer (KAPA Biosystems), 3 μL of a mix comprising 10 mM dNTPs (KAPA Biosystems), 3 μL of 100 μM P5RP1 primer, 3 μL of 100 μM EP7v2 primer listed in Tables S5, and 2 μL of 1 U/μL KAPA HiFi HotStart DNA polymerase (Roche). The 25-μL mixture of 5′-end-filled cDNAs and the beads was transferred into a new 0.2-mL PCR tube and mixed with 75 μL of PCR mix3 and centrifuged briefly. The beads were re-suspended by pipetting, after which the tubes were immediately set on a thermal cycler and a PCR was performed using the following conditions: an initial denaturation at 95°C for 2 min; followed by 10 cycles of 98°C for 20 s, 63°C for 30 s, and 72°C for 30 s; with a final extension at 72°C for 5 min, after which the samples were stored at 4°C. The enriched libraries were purified with a MinElute PCR purification kit and eluted with 28 μL of EB, according to the manufacturer's instructions. The NGS libraries were then subjected to size selection, where fragments measuring 300 bp to 800 bp were electrophoretically recovered from the enriched NGS libraries using BluePippin (Sage Science) with a 1.5% dye-free agarose gel cassette and the internal standard R2, according to the manufacturer's instructions. Size-selected NGS libraries were purified with a MinElute PCR purification kit and eluted in 28 μL of EB, according to the manufacturer's instruction. The quantity and quality of the NGS libraries were determined using a Bioanalyzer 2100 with a High Sensitivity DNA kit.

Wishbone – Seurat – PeakMatch pipeline

To identify scRNA-seq data related to the xylem cell lineage, Wishbone was performed as previously described (Setty et al., 2016). Samples after differentiation induction in VISUAL were subjected to Wishbone. The first and third components of principal component analysis (PCA) were used for t-SNE. The xylem lineage was selected according to the expression of xylem cell marker genes on the t-SNE plots.

Clustering of cells was performed using the Seurat R package (Satija et al., 2015). In brief, digital gene expression matrices were column-normalized and log-transformed. To obtain a landmark gene set for Seurat, we divided all genes in cpRNA-seq data into 17

groups according to the peak expression time of each gene. The 17 genes showing the highest correlation coefficient with scRNA-seq data in each respective group were selected as landmark genes. In addition to the 17 genes, cell-type-specific markers (*CAB3*, *LHCB2.1*, *TDR*, *AtHB8*, *IRX3*, *IRX8*, and *SEOR1*) were also selected as landmark genes. In total, 24 genes were used as a landmark gene set for Seurat.

Finally, we selected the genes whose correlation coefficient between the expression pattern in scRNA-seq and cpRNA-seq was more than 0.5. Among the selected genes, 2,217 genes, which are expressed in at least 10 single cells were subjected to PeakMatch with the following parameters: T = 1, last = 0, intv = 1, inter = 7.

Overview of the PeakMatch algorithm

Let $_Z$ be the set of whole genes under consideration. Discretizing pseudo and actual times into integers for simplicity, we denote by $P = \{1,\ldots,m\}$and $A = \{1,\ldots,n\}$ the sets of available pseudo and actual times, respectively. Suppose that, for each gene $z \in Z$, we are given pseudo time-series based scRNA-seq data $S_Z = (S_{Z,1},\ldots S_{Z,m})$ and actual time-series based cpRNA-seq data $C_Z = (c_{z,1},\ldots,c_{z,n})$, where $S_{z,p} \in S_z$ and $c_{z,a} \in C_z$ represent the gene z's expression levels at a pseudo time p in the scRNA-seq data, and at an actual time a in the cpRNA-seq data, respectively.

To estimate the actual times of gene expressions in the scRNA-seq data, we would like to find pairs $(p,a) \in P \times A$ of pseudo and actual times so that the expression levels $S_{z,p}$ and $C_{z,a}$ are likely to be "comparable" for many genes $z \in Z$. Once such pairs (p,a) are found, we may estimate the actual time of $S_{z,p}$ by that of $C_{z,a}$.

The point is that, among the observed gene expression levels, "peaks" are the most important phenomena. Then it is desired that a peak in S_Z and a peak in C_Z should be matched. It is also required that the pseudo time order should be preserved in the time pairs. To be more precise, whenever a pseudo time p is matched to an actual time a, any pseudo time $p' > p$ should be matched to an actual time $a' > a$.

We formulated the problem of finding such time pairs as the maximum weighted non-crossing matching (MWNCM) problem for a bipartite graph. The problem is polynomially solvable (Malucelli et al., 1993), meaning that it is efficiently solvable from the standpoint of the theory of computational complexity.

We took the bipartite graph so that one vertex subset was the pseudo time set P and the other vertex subset was the actual time set A. For the edge set, we considered all possible pairs $(p,a) \in P \times A$, where we determined the weight of an edge (p,a) heuristically by how the pseudo time p and the actual time a were comparable peaks. We determined the weight of an edge (p,a) as follows. For each gene $z \in Z$, we decided whether or not the value $s_{z,p}(resp.,c_{z,a})$ was within a "peak area" in $S_z(resp.,C_z)$. We considered that $s_{z,p}(resp.,c_{z,a})$ was within a peak area if it was significantly larger than a general trend of $S_z = (s_z,1,\ldots,s_{z,m})$ (resp., $C_z = (c_{z.1},\ldots,c_{z,n})$), which was estimated by an exponential moving average. We set the weight of (p,a) to a larger value if both $S_{z,p}$ and $C_{z,a}$ are among peak areas for more genes.

Given the scRNA-seq and cpRNA-seq data, the algorithm PeakMatch constructed the bipartite graph, derived an MWNCM for it, and estimated the actual times of all pseudo times in P based on the derived MWNCM.

For more details and python-based programs, see https://github.com/endo-lab/PeakMatch.

Performance comparison of PeakMatch algorithm

Performance was evaluated using scRNA-seq and cpRNA-seq data provided by the present study and the previous report (Sun et al., 2017). Both data sets were subjected to PeakMatch and iCpSc (Sun et al., 2017) with default parameters. Data in SingleCells.cpDEGs_selected_big32none0_overlap.txt was used as the output of iCpSc. The data used in the previous report (Sun et al., 2017) was downloaded from GitHub (https://github.com/AHallLab/PredictingCircadianTime).

Plasmid construction

For *IRX3*::*GUS*, the promoter of *IRX3* was amplified from Col-0 genomic DNA using the oligonucleotide primers listed in Table S5. The amplified fragment was cloned into the XhoI site of pENTR1A (no ccdB). After sequence verification, this plasmid was recombined with pGWB3 (Nakagawa et al., 2007), and introduced into Col-0 plants.

For *35S*::*LHY*, the coding regions of *LHY* gene was amplified from cDNA derived from Col-0 plants using the oligonucleotide primers listed in Table S5. The amplified *LHY* cDNA was cloned into the pENTR/D-TOPO vector. After sequence verification, this plasmid was recombined with pFAST-G02 (Shimada et al., 2010), which contains the CaMV 35S promoter-driven expression cassette, and introduced into Col-0 plants.

For *BES1*::*BES1-GFP*, the genomic DNA fragment of BES1 containing the 2 kb promoter sequence and the 1 kb downstream sequence from the stop codon was amplified from Col-0 genomic DNA using the oligonucleotide primers listed in Table S5. The amplified fragment was cloned into the pENTR/D-TOPO (Thermo Fisher Scientific). After sequence verification, this plasmid was recombined with pGWB1 (Nakagawa et al., 2007). The resulting pGWB1-gBES1 was linearized by PCR using the oligonucleotide primers listed in Table S5. Then, sGFP fragment was amplified using the oligonucleotide primers listed in Table S5. The sGFP fragment was inserted just before the stop codon of BES1 by fusion of the two fragments using In-Fusion HD Cloning Kit. After sequence verification, this plasmid was introduced into the *bes1-3* mutant.

For luciferase reporter constructs, the NOS terminator was amplified by PCR using the oligonucleotide primers listed in Table S5. The amplified fragment was cloned into the XbaI site of pENTR1A (no ccdB) using an In-Fusion HD Cloning Kit (TaKaRa). In the same

way, the coding sequence of LUC+ was amplified and cloned into the XhoI-EcoRV site of the plasmid using the oligonucleotide primers listed in Table S5. The resulting pENTR1A (LUC-nosT) was used for *LHY*::*LUC*. The promoter of *LHY* was amplified from Col-0 genomic DNA using the oligonucleotide primers listed in Table S5. The amplified fragment was cloned into the XhoI site of pENTR1A (LUC-nosT). After sequence verification, the plasmid was recombined with pFAST-G01 (Shimada et al., 2010), introduced into Col-0 plants, and transgenic plants were selected by fluorescence of T1 seeds.

For transactivation assay constructs, the coding sequences of *bes1-D*(L) from cDNA of the *bes1-D* mutant and *RLUC* from the vector pRL vector (Promega) were amplified by PCR using the oligonucleotide primers listed in Table S5. The amplified fragments were cloned into the BamHI site of pPZP211/NP/35S-nosT (Nishimura et al., 2003) using an In-Fusion HD Cloning Kit.

Western blotting

Plants expressing *BES1*::*BES1-GFP* were harvested every 8 h from 24 h before up to 72 h after differentiation induction in VISUAL. Approximately 50 mg of seedlings were ground into a fine powder in liquid nitrogen with a mortar and pestle, mixed with equal volumes of 2×Laemmli sample buffer (100 mM Tris-HCl(pH 6.8), 4%(w/v) SDS, 10%(v/v) 2-mercaptoethanol, and 20%(v/v) glycerol) and boiled at 95°C for 5 min. Samples were separated by SDS-PAGE on a 7.5% acrylamide gel, and transferred onto polyvinylidene fluoride membranes (Bio-Rad Laboratories). For the primary antibody, polyclonal anti-GFP (MBL-598) was diluted 1:2,000. For the secondary antibody, ECL Rabbit IgG, HRP-linked whole Ab (GE Healthcare) was diluted 1:10,000. Blots were visualized with ECL Prime reagent (GE Healthcare) and ImageQuant LAS 4010 (GE Healthcare).

ChIP-qPCR and ChIP-seq

Chromatin immunoprecipitation assays using *BES1*::*BES1-GFP*/*bes1-3* and *LUX*::*LUX-GFP*/*lux-4* were performed as described (Yamaguchi et al., 2014) with modifications. Briefly, 600 mg of seedlings at 8 h (for *BES1*::*BES1-GFP*/*bes1-3*) or 24 h (*LUX*::*LUX-GFP*/*lux-4*) after differentiation induction in VISUAL were fixed in PBS containing 1% paraformaldehyde for 10 min at room temperature, and nuclei and chromatin were isolated. The isolated chromatin was sheared with a Covaris S220 sonicator under these parameters: 4–6°C, 175 W peak power, 5% duty factor, 200 cycles/burst, for 50 s of treatment. To immunoprecipitate chromatin, 10 μL of anti-GFP antibody (MBL-598) and 50 μL of Dynabeads Protein G (Thermo Fisher Scientific) were used. The precipitated samples were subjected to qPCR or library preparation for ChIP-seq. MYB30 (Li et al., 2009) was used as a positive control for ChIP with BES1. For ChIP-qPCR, specific sequences for each primer pair were listed in Table S5. The following thermal cycling profile was used for all the primers: 95°C for 60 s, ~40 cycles of 95°C for 10 s, 60°C for 45 s.

For ChIP-seq, the sequence libraries were prepared using a TruSeq ChIP Sample Preparation Kit (Illumina), and sequenced using an Illumina NextSeq 500 system with a 75-nt single-end sequencing protocol. The sequence reads were mapped to the TAIR10 *Arabidopsis* genome sequence by HISAT2 (Kim et al., 2015) with default parameters. Peaks were identified by MACS2 (Zhang et al., 2008), using the matching INPUT control with the genome size parameter "-g 1.3e8".

Transactivation assay

Agrobacterium cultures carrying plasmids for the transactivation assay were grown overnight at 28°C, collected by centrifugation, and adjusted to an OD600 of 0.4 with infiltration buffer (10 mM MES(pH 5.6), 10 mM $MgCl_2$, 150 μM acetosyringone, and 0.02% Silwet-L77). Cells were kept at 28°C in the dark for 1 to 2 h and then infiltrated into the abaxial air spaces of 4-week-old *N. benthamiana* plants grown under 12L/12D conditions at ZT0. After infiltration, plants were kept under 12L/12D conditions for 36 h and harvested at ZT12. The transactivation assay was performed with a Dual-Luciferase Reporter Assay System (Promega) according to the manufacturer's instructions.

Detection of bioluminescence

For detection of bioluminescence in seedlings, a surface sterilized seed was sown to the liquid medium as described previously (Kondo et al., 2016), supplemented with 0.025 mM luciferin (Biosynth), and incubated under continuous light conditions for 6 days. For detection of bioluminescence during VISUAL, a cotyledon of a 7-day-old plant grown under 12L/12D conditions was transferred to the liquid medium as described previously (Kondo et al., 2016), supplemented with 0.025 mM luciferin at ZT0, and incubated under 12L/12D conditions for 2 days. Then, the cotyledon was transferred to the liquid medium for vascular cell differentiation, containing 0.025 mM luciferin at ZT0 and incubated under LL conditions for 3 days. For photon counting, the emitted luminescence was recorded using a photomultiplier-tube-based bioluminescence monitoring system (Golden et al., 1997).

QUANTIFICATION AND STATISTICAL ANALYSIS

Measurement of xylem cell induction ratio

Plants were fixed in acetic ethanol fixative (75% glacial acetic acid and 25% ethanol) for 1 day, stained with 20% phloroglucinol in 99.5% ethanol and concentrated HCl (1:19, v/v) for 1 h, cleared with chloral hydrate/glycerol/H_2O mixture (8 g of chloral hydrate in 1 mL of glycerol and 2 mL of H_2O) for 2 h, and observed under a light microscope. For quantification of the xylem cell induction ratio, areas for lignin-stained xylem cells or lignin autofluorescence in the cotyledons were manually calculated using the polygon selection tool implemented in ImageJ.

Measurement of stomatal index and root length

For measurement of stomatal index, 10-day-old plants grown under 12L/12D conditions were stained with 50 μg/mL of propidium iodide (PI) and observed using a confocal laser scanning microscope, FV1000 (Olympus) in three square areas of 0.48 mm^2 per cotyledon from 5 cotyledons of 5 independent plants. The stomatal index was calculated as previously described (Kang et al., 2009). Error bars, representing standard errors, were calculated from the results of 5 independent cotyledons.

For root length measurements, plants were grown vertically under 12L/12D conditions. Root length was measured at ZT0.